Linchpin DNA-binding residues serve as go/no-go controls in the replication factor C-catalyzed clamp-loading mechanism

Received for publication, May 24, 2017, and in revised form, August 2, 2017 Published, Papers in Press, August 14, 2017, DOI 10.1074/jbc.M117.798702

Juan Liu, Yayan Zhou, and Manju M. Hingorani[1]

From the Department of Molecular Biology and Biochemistry, Wesleyan University, Middletown, Connecticut 06459

Edited by Patrick Sung

DNA polymerases depend on circular sliding clamps for processive replication. Clamps must be loaded onto primer–template DNA (ptDNA) by clamp loaders that open and close clamps around ptDNA in an ATP-fueled reaction. All clamp loaders share a core structure in which five subunits form a spiral chamber that binds the clamp at its base in a twisted open form and encloses ptDNA within, while binding and hydrolyzing ATP to topologically link the clamp and ptDNA. To understand how clamp loaders perform this complex task, here we focused on conserved arginines that might play a central coordinating role in the mechanism because they can alternately contact ptDNA or Walker B glutamate in the ATPase site and lie close to the clamp loader–clamp-binding interface. We mutated Arg-84, Arg-88, and Arg-101 in the ATPase-active B, C, and D subunits of *Saccharomyces cerevisiae* replication factor C (RFC) clamp loader, respectively, and assessed the impact on multiple transient events in the reaction: proliferating cell nuclear antigen (PCNA) clamp binding/opening/closure/release, ptDNA binding/release, and ATP hydrolysis/product release. The results show that these arginines relay critical information between the PCNA-binding, DNA-binding, and ATPase sites at all steps of the reaction, particularly at a checkpoint before RFC commits to ATP hydrolysis. Moreover, their actions are subunit-specific with RFC-C Arg-88 serving as an accelerator that enables rapid ATP hydrolysis upon contact with ptDNA and RFC-D Arg-101 serving as a brake that confers specificity for ptDNA as the correct substrate for loading PCNA.

Sliding clamps encircle DNA and function as mobile tethers for polymerases, thereby enabling processive DNA synthesis at the rate of hundreds of nucleotides per second required for genome duplication (1, 2). Clamps must be loaded onto DNA to serve their purpose, and this task is performed by clamp loaders in an ATP-fueled reaction (Fig. 1*A*) (3, 4). In addition to their essential role as processivity factors, clamps also enable and coordinate the actions of many proteins involved in DNA replication, repair, recombination, chromatin remodeling, and other DNA metabolic processes as well as cell cycle control. Unsurprisingly, clamps and clamp loaders are highly conserved through evolution, and defects in their function are associated with cancer and other disease states (5, 6).

The core structural features of clamps and clamp loaders are quite similar in organisms across all branches of life. Clamps are formed by two or three subunits arranged in a planar ring, each containing multiple β-α-β domains with β sheets forming the outer rim plus interfaces between subunits and α helices forming the inner rim that presents positively charged residues toward the DNA enclosed within (7–10). Clamp loaders are formed by five subunits (A–E), also arranged in a ring except for a gap between the A and E subunit N-terminal domains, essentially creating a chamber with a closed roof and a slightly open doorway (Fig. 1*B*). Each subunit comprises three domains: the N-terminal domains I and II form the signature module of the AAA+ ATPase protein family and the C-terminal domain III forms a closed collar through interactions with the other subunits (11–13). The core clamp-loading mechanism is also quite similar among bacteriophage, bacterial, archaeal, and eukaryotic clamp loaders examined thus far: ATP binding activates the clamp loader to bind and open the clamp and place primer–template DNA (ptDNA)[2] within, whereas ATP hydrolysis triggers ring closure and release of the topologically linked clamp-DNA product (Fig. 1) (3, 14).

Transient kinetic studies of eukaryotic RFC (15–19), *Escherichia coli* γ/τ complex (20–23) and bacteriophage T4 gp44/62 (24–26) clamp loaders have revealed an intricate, multistep reaction mechanism, and the current model for *Saccharomyces cerevisiae* RFC, the subject of this study, is outlined below (15–18, 27, 28). Binding of two to three ATP molecules to RFC initiates a relatively slow process of activation during which the clamp loader binds a PCNA clamp with high affinity, which in turn accelerates activation. During this process, RFC binds an additional one to two ATP molecules and stabilizes PCNA in an open spiral conformation. This RFC-ATP-PCNA$_{open}$ complex can bind ptDNA rapidly and with high affinity. Interaction with DNA triggers further activation of RFC that results in a burst of ATP hydrolysis by three subunits, likely B, C, and D, by analogy to the three ATPase-active γ subunits in *E. coli* γ complex. ATP hydrolysis initiates a relatively slow process of RFC deactivation

This work was supported by National Institutes of Health Grant R15 GM114743 (to M. M. H.). The authors declare that they have no conflicts of interest with the contents of this article. The content is solely the responsibility of the authors and does not necessarily represent the official views of the National Institutes of Health.

This article contains a supplemental movie and Figs. S1–S6.

[1] To whom correspondence should be addressed. Tel.: 860-685-2284; E-mail: mhingorani@wesleyan.edu.

[2] The abbreviations used are: ptDNA, primer–template DNA; PCNA, proliferating cell nuclear antigen; RFC, replication factor C; TAMRA, 5-(and 6)-carboxytetramethylrhodamine; MDCC, 7-diethylamino-3-((((2-maleimidyl) ethyl)amino)carbonyl) coumarin; AF, Alexa Fluor 488; PBP, phosphate-binding protein; ATPγS, adenosine 5′-*O*-(3′-thiotriphosphate); ssDNA, single-stranded DNA; nt, nucleotide.

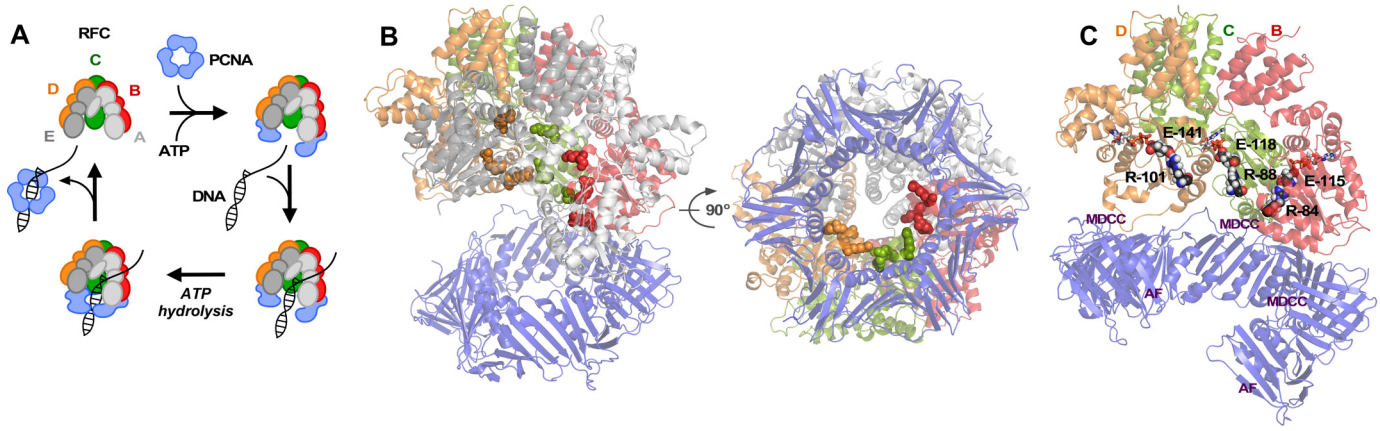

Figure 1. Select DNA-binding residues involved in RFC-catalyzed PCNA loading on DNA. *A*, main stages of the clamp-loading reaction. *B*, front and bottom views of the RFC-ATPγS-PCNA$_{closed}$ complex (Protein Data Bank code 1SXJ (12)) showing RFC subunits A (*light gray*), B (*red*), C (*green*), D (*orange*), and E (*dark gray*) and PCNA (*blue*) and highlighting DNA-binding residues as *spheres* in subunits B (Arg-84, Arg-90, and Lys-149), C (Arg-88, Arg-94, and Lys-152), and D (Arg-101, Arg-107, and Arg-175). *C*, a model of RFC-ATPγS-PCNA$_{open}$ complex derived from Protein Data Bank code 1SXJ (35) showing arginines RFC-B Arg-84, RFC-C Arg-88, and RFC-D Arg-101 (mutated to alanine in this study) in contact with ATPase site Walker B glutamates RFC-B Glu-115, RFC-C Glu-118, and RFC-D Glu-141, respectively (ATPγS shown as *sticks* in each site; see supplemental movie). *MDCC* (three dyes) and *AF* (one of three dye pairs at subunit interfaces) denote dye locations on PCNA.

during which the clamp loader loses affinity for ptDNA and PCNA, allowing clamp closure around ptDNA and phosphate release, followed by release of the PCNA-ptDNA complex and ADP and catalytic turnover (15–18, 27, 28).

Structural studies of clamps and clamp loaders from various organisms illustrate some of the reaction mechanics. As in other oligomeric AAA+ family proteins (29), nucleotide-binding sites are located at the interfaces between clamp loader subunits with Walker A and B motifs in one subunit and the SRC motif/arginine finger presented by a neighboring subunit to enable catalysis (3). Three ATPase sites, located at the central B, C, and D subunits, appear to be essential for clamp loading. In T4 gp44/62, the A subunit lacks an AAA+ module, and the E subunit lacks a trans-acting SRC motif; therefore, they are ATPase-inactive (13). In *S. cerevisiae* RFC, all five subunits contain the Walker A motif for ATP binding, but the Walker B catalytic glutamate is mutated in RFC-E, and there is no trans-acting SRC motif to activate ATP hydrolysis (12); RFC-A hydrolyzes ATP, but it has the least significant role in the reaction (27) and appears to mainly facilitate catalytic turnover after PCNA is loaded onto ptDNA (30). Finally, as noted above, the *E. coli* clamp loader has only three ATPase active γ/τ subunits (11). ATP analog-bound structures of *S. cerevisiae* RFC, *E. coli* γ complex, and T4 gp44/62 show the AAA+ modules arranged in a right-handed spiral (12, 13, 31). Clamps also have the propensity to transiently twist open out of plane (32–34). Interactions between the clamp and the base of the clamp loader stabilize both in a spiral conformation that complements the DNA helix (13, 35). This is likely the ATP binding- and clamp-induced active RFC-ATP-PCNA$_{open}$ state identified in the kinetic mechanism above. Note that the RFC-ATPγS-PCNA structure shown in Fig. 1*B* features a closed clamp that contacts only the lower arm of the RFC spiral (RFC-A, RFC-B, and RFC-C subunits) (12), but a computationally derived model with open PCNA (Fig. 1*C*) recapitulates the spiral conformation of both proteins in the gp44/62 clamp loader-gp45 open clamp crystal structure (35).

The γ complex and gp44/62 structures confirmed that ptDNA is bound with the duplex enclosed within the clamp loader chamber and the single-stranded template extruding from the gap between δ (A) and δ′ (E) subunits in γ complex (31) and between two domains of the A subunit in gp44/62 (13). Both the clamp loader and clamp have positively charged surfaces on the inside for interaction with the duplex. In *S. cerevisiae* RFC, N-terminal dipoles of three α helices in each subunit (α4–6) as well as multiple lysine and arginine residues point into the chamber and track the DNA backbone (12). These features are common to clamp loaders in all domains of life. An RFC mutant in which the conserved residues in subunits RFC-B (Arg-84, Arg-90, and Lys-149), RFC-C (Arg-88, Arg-94, and Lys-152), and RFC-D (Arg-101, Arg-107, and Arg-175) were all replaced with alanine could not bind ptDNA or load PCNA, reflecting the importance of this DNA-interacting surface (Fig. 1*B*) (36). Mutations of analogous residues in *E. coli* γ complex also disrupt ptDNA binding and clamp loading (37). The clamp also has several conserved basic residues lining the inside of the ring (7, 9), and in a previous kinetic study with *S. cerevisiae* PCNA, we showed that loss of even one can alter the rates of all DNA-dependent steps in the reaction (16). In the presence of ptDNA, the spiral symmetry of the AAA+ modules is tighter, which improves the complementarity of the clamp loader–open clamp interface and, importantly, organizes the ATPase sites into a catalytically competent state with the Walker B glutamate and the SRC arginine finger positioned for ATP hydrolysis (13, 31). This is likely the ptDNA binding-induced active RFC-ATP-PCNA$_{open}$-ptDNA state that undergoes a burst of ATP hydrolysis in the kinetic mechanism outlined above. In a gp44/62-gp45 structure with ADP bound to the B subunit, the spiral symmetry of the AAA+ modules is disrupted and the subunit is disengaged from DNA as well as gp45, which is closed (13). This structure may reflect a state during RFC deactivation after ATP hydrolysis and phosphate release that results in PCNA-ptDNA release in the kinetic mechanism outlined above.

A

PCNA^{MDCC} binding (ATP, no ptDNA)	k_{on} nM^{-1}s^{-1}	k_{off} s^{-1}	K_D nM
RFC$_{WT}$	1 ± 0.03	0.02 ± 0.0001	0.02
RFC-B$_{R84A}$	0.9 ± 0.03	0.08 ± 0.0002	0.09
RFC-C$_{R88A}$	0.9 ± 0.03	0.05 ± 0.0002	0.06
RFC-D$_{R101A}$	1.3 ± 0.04	0.03 ± 0.0001	0.02
RFC-BCD$_{AAA}$	0.9 ± 0.03	0.18 ± 0.0007	0.2

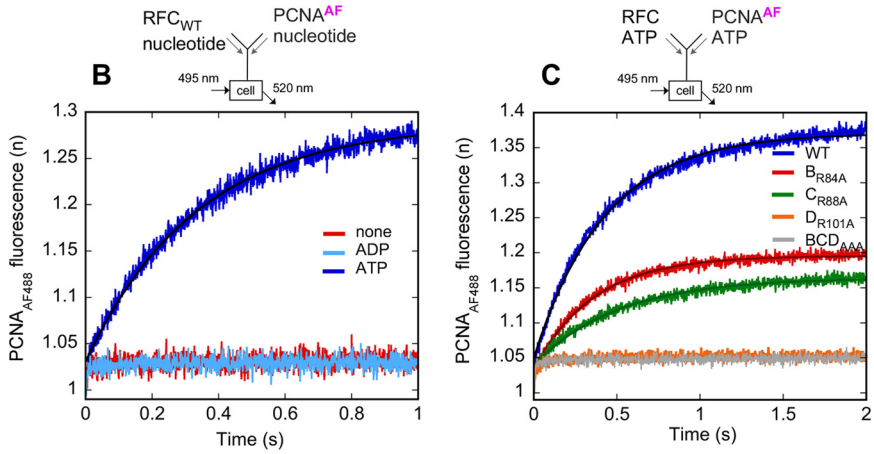

Figure 2. Arginine mutants exhibit RFC subunit-specific defects in ATP-induced, DNA-independent PCNA binding and opening. *A*, PCNA binding was measured by fluorescence increase over time on mixing PCNA^{MDCC} with wild-type or mutant RFC in the presence of ATP (final concentrations: 0.1–0.4 μM RFC, 0.02 μM PCNA^{MDCC}, and 0.5 mM ATP), and dissociation by signal decrease on mixing RFC, PCNA^{MDCC}, and ATP with excess unlabeled PCNA (final concentrations: 0.2 μM RFC, 0.02 μM PCNA^{MDCC}, 0.5 mM ATP, and 1 μM PCNA). The table lists rates from a single-exponential fit of the data (supplemental Fig. S1). *B* and *C*, PCNA opening was measured by signal increase over time on mixing PCNA^{AF} and RFC in the presence of ADP or ATP (final concentrations: 0.2 μM RFC, 0.02 μM PCNA^{AF}, and 0.5 mM ATP or ADP); the data were fit to a single-exponential function. Wild-type RFC opens PCNA in an ATP-dependent manner at 2.3 ± 0.02 s^{-1}, and the mutants exhibit varying defects: RFC-B^{R84A} and RFC-C^{R88A} are able to partially open the clamp (at 2.8 ± 0.02 and 2 ± 0.03 s^{-1}, respectively), whereas RFC-D^{R101A} and the RFC-BCD^{AAA} triple mutant appear unable to do so.

We are interested in understanding how the various activities involved in getting a circular clamp around DNA are coordinated, *i.e.* how (*a*) clamp binding/opening/closing/release, (*b*) ptDNA binding/release, and (*c*) ATP binding/hydrolysis/product release are coupled with each other. Structural analysis of gp44/62 led to an interesting "switch" hypothesis about ptDNA-induced ATP hydrolysis based on the conformation of a conserved DNA-binding residue that lies close to the Walker B glutamate. In the absence of ptDNA, Lys-80 in gp44/62 B, C, D, and E subunits contacts the glutamate backbone, potentially holding this catalytic residue in an inactive conformation. In the presence of ptDNA, Lys-80 contacts the DNA backbone instead. This switch in Lys-80 position may allow the glutamate to adopt an active conformation that facilitates attack of water on ATP (13, 38). Mutation of the corresponding Lys-100 in *E. coli* γ complex slightly increases the ATPase k_{cat} (37), supporting the idea that the switch residue inhibits ATP hydrolysis until it moves away to bind ptDNA. Notably, in addition to linking the DNA-binding and ATPase sites as proposed above, the residue lies in a loop just preceding the PCNA-binding α helix (α4). We therefore considered the possibility that it serves as a link between all three active sites during the clamp-loading reaction. To test this hypothesis, we mutated the corresponding residues, individually and together, in the three *S. cerevisiae* RFC subunits with essential ATPase activity: RFC-B (R84A), RFC-C (R88A), and RFC-D (R101A) (Fig. 1*C* and supplemental movie). The effects of these mutations on coordination between the PCNA-binding, ptDNA-binding and ATPase sites were assessed by monitoring several transient events in the reaction during which transactions of RFC with one ligand influence the others.

The results reveal that the ATPase-triggering mechanism is more complex than perceived by the switch hypothesis because arginine removal did not lead to unregulated, ptDNA-independent ATP hydrolysis by RFC. However, these residues do exert significant control on how PCNA, ptDNA, and ATP are processed through the reaction. Moreover, their role depends on the clamp loader subunit; thus, Arg-84, Arg-88, and Arg-101 in RFC-B, RFC-C, and RFC-D, respectively, are increasingly important for stabilization of open PCNA upon ATP binding to RFC; Arg-88 in RFC-C is important for efficient positioning of ptDNA in the complex, which in turn enables further PCNA opening, ATP hydrolysis, and completion of loading; and Arg-101 in RFC-D is important for choosing ptDNA as the correct substrate to load PCNA.

Results

The locations of the three arginines selected for investigation, Arg-84 (RFC-B), Arg-88 (RFC-C), and Arg-101 (RFC-D), suggest that they are involved in RFC transactions with all three ligands, PCNA, ptDNA, and ATP, during the course of the clamp-loading reaction. Their specific mechanistic roles were investigated by testing the impact of mutation to alanine on individual steps in the reaction. The following sections recount results from transient kinetic measurements of PCNA binding/opening/closure/release, ptDNA binding/release, and ATP hydrolysis/product release, any or all of which could potentially be altered in the mutant proteins.

The lower spiral arm of RFC (RFC-B Arg-84) is important for binding PCNA

Previous studies have shown that RFC can bind and open PCNA-absent ptDNA (15, 39, 40); hence the mutants were tested first for this activity. RFC binding to PCNA^{MDCC} results in an increase in fluorescence, and this signal was monitored over time after mixing the proteins on a stopped-flow instrument (PCNA is labeled at S43C with 7-diethylamino-3-((((2-maleimidyl)ethyl)amino)carbonyl) coumarin (MDCC); Ref. 39). Wild-type RFC binds PCNA rapidly on the order of 10^9 M^{-1} s^{-1} in the absence or presence of ATP (Fig. 2*A* and supplemental Fig. S1, A and B) All four mutants, RFC-B^{R84A}, RFC-C^{R88A}, RFC-D^{R101A}, and RFC-BCD^{AAA}, also bind PCNA

at similar rates in the absence or presence of ATP. Mixing wild-type or mutant RFC-PCNA^{MDCC} complex preformed without ATP and unlabeled PCNA chase showed that the complex dissociates rapidly at rates of 30–45 s^{-1} (supplemental Fig. S1C, table). The resulting K_D is ~50 nM for all RFCs, indicating that the point mutations do not cause gross alterations in RFC structure or its PCNA-binding interface. With ATP, the rate of PCNA dissociation from wild-type RFC slows ~1500-fold to 0.02 s^{-1}, yielding a very tight K_D of 0.02 nM (Fig. 2*A* and supplemental Fig. S1D, table); this value is ~100-fold lower than reported previously from equilibrium measurements (18, 39), possibly because those reactions contained significant levels of ADP produced by RFC. As noted earlier, ATP binding promotes a spiral conformation of RFC, and these results show that ATP-induced extension of the binding interface between RFC and PCNA increases their affinity by well over 1000-fold. ATP binding also stabilizes PCNA interaction with all of the RFC mutants, but the dissociation rate is faster and results in progressively lower affinity for RFC-D^{R101A} (similar to wild type), RFC-C^{R88A}, RFC-B^{R84A}, and RFC-BCD^{AAA} (Fig. 2*A* and supplemental Fig. S1D, table). The mutations perturb RFC-PCNA interaction either directly by altering the nearby binding interface or indirectly by altering the Walker B glutamate position and thereby the effects of ATP binding to RFC (28). The graded effect indicates that PCNA contact with the lower arm of the RFC spiral is more important for complex formation than that with the upper arm (consistent with the RFC-ATPγS-PCNA crystal structure; Ref. 12).

The upper spiral arm of RFC (RFC-D Arg-101) is important for holding PCNA open before ptDNA binding

Opening of PCNA^{AF} results in an increase in fluorescence, and this signal was monitored over time after mixing the clamp with RFC on a stopped-flow (PCNA is labeled at I111C and I181C with Alexa Fluor 488, and dye proximity in the closed clamp results in self-quenching; Ref. 39). Wild-type RFC requires ATP to open PCNA at a rate of 2.3 s^{-1} (Fig. 2*B*) as reported previously (16, 39, 40). The rate is independent of RFC concentration (data not shown), and since RFC binds PCNA rapidly (200 s^{-1} at 0.2 μM), the slow rate reflects PCNA opening after initial RFC-ATP-PCNA complex formation. The arginine mutants are defective in PCNA opening, and the gradation is the reverse of that observed for PCNA binding; *i.e.* opening is progressively worse with RFC-B^{R84A}, RFC-C^{R88A}, and RFC-D^{R101A} (Fig. 2*C*); RFC-BCD^{AAA} remains the worst affected. The results indicate that contact with the upper arm of the RFC spiral is more important for PCNA opening than that with the lower arm. The results are also consistent overall with a prior study in which mutation of the SRC arginine finger in RFC-C and RFC-D ATPase sites is more disruptive to PCNA opening than in RFC-B (30). Together the PCNA binding and opening data indicate that RFC-B Arg-84 is important for complex formation between RFC and PCNA, whereas RFC-D Arg-101 is an important anchor for stabilizing PCNA in open form (Fig. 1, *B* and *C*). It is striking that residues identified primarily as contact points between RFC and ptDNA have such a substantive role in ptDNA-independent, ATP-induced PCNA binding and opening. This finding supports our hypothesis that the location of these arginines, proximal to the ATPase site catalytic glutamate and the PCNA-binding helix in RFC, bodes a central coordinating role in the reaction mechanism.

RFC-C Arg-88 and RFC-D Arg-101 promote ptDNA binding and positioning within the RFC-ATP-PCNA complex

ATP binding enables the clamp loader to bind ptDNA, and this interaction was monitored by change in ptDNA^{TAMRA} fluorescence, first under equilibrium conditions with non-hydrolyzable ATPγS (ptDNA is labeled at the 3′ primer end with 5-(and 6-)carboxytetramethylrhodamine; TAMRA). Titration with wild-type RFC in the absence of PCNA yielded a K_D of 1.8 nM (supplemental Fig. S2A, table), which is comparable with prior results with ptDNA^{TAMRA} and [^{32}P]ptDNA filter-binding assays (15, 41). RFC-B^{R84A} and RFC-C^{R88A} exhibit similar affinity for ptDNA as wild-type RFC, whereas RFC-D^{R101A} binding is 4-fold weaker, suggesting that the RFC-D subunit has a more significant role in the interaction; RFC-BCD^{AAA} has no detectable interaction. The amplitude of the signal is lower for all single mutants (65–75% of wild type), suggesting a smaller fraction of bound ptDNA or perhaps differences in mutant *versus* wild-type RFC-ATPγS-ptDNA^{TAMRA} complex conformations (supplemental Fig. S2A). The effect of PCNA on the interaction was measured next by stopped-flow experiments in which RFC, ATPγS, and PCNA were mixed with ptDNA^{TAMRA} and monitored over time. PCNA facilitates ptDNA binding because the signal now approaches that of wild-type RFC for all single mutants, indicating that they achieve the same bound fraction and conformation (Fig. 3*A*); RFC-BCD^{AAA} can also bind ptDNA, albeit very slowly, in the presence of PCNA, and the signal saturates at ~75% of wild type in 60 s (data not shown). RFC-B^{R84A}, RFC-C^{R88A}, and RFC-D^{R101A} exhibit increasingly longer lag phases and times to saturation, indicating that these mutations slow down formation of the ATP-bound RFC-PCNA$_{open}$-ptDNA complex. As observed with PCNA opening (Fig. 2*C*), RFC-D has the most significant and RFC-B has the least significant role in the interaction between RFC and ptDNA.

ptDNA binding was monitored next under clamp-loading conditions by double mixing stopped-flow experiments in which RFC and PCNA were premixed with ATP for 3 s to complete clamp opening (Fig. 2*B*) followed by addition of ptDNA^{TAMRA} to the reaction. We observed initial rapid quenching of TAMRA fluorescence with rates dependent on RFC concentration (Fig. 3*B*, *inset*). This phase yields a bimolecular binding rate constant of 1×10^9 M^{-1} s^{-1} for formation of an RFC-ATP-PCNA$_{open}$-ptDNA collision complex (Fig. 3*D*). RFC-B^{R84A} and RFC-C^{R88A} exhibit similar ptDNA-binding rates as wild-type RFC, RFC-D^{R101A} is 4-fold slower, and RFC-BCD^{AAA} is at least 10-fold slower (supplemental Fig. S2B and Fig. 3*D*). There is a subsequent increase in fluorescence that is independent of RFC concentration and occurs at 20 s^{-1} with wild-type protein (Fig. 3, *B* and *D*) Given a similar signal increase with non-hydrolyzable ATPγS (albeit slower at 3.5 s^{-1}; Fig. 3*A*), we interpret that the second phase reports an intramolecular conformational change after initial ptDNA binding but prior to ATP hydrolysis. This isomerization (reported by TAMRA at the 3′ primer end) could be adjustment of the

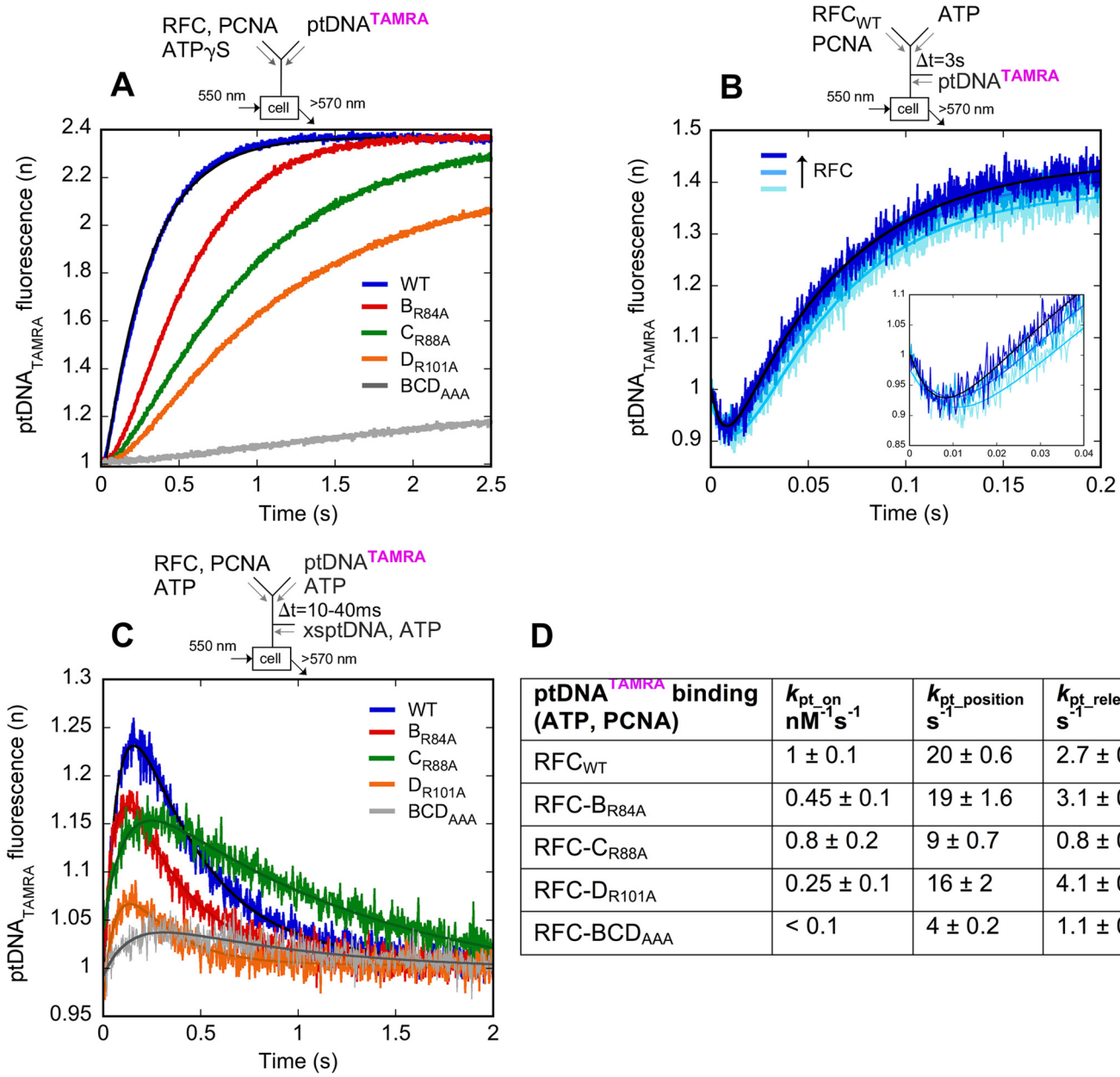

ptDNA^{TAMRA} binding (ATP, PCNA)	k_{pt_on} nM^{-1}s^{-1}	$k_{pt\_position}$ s^{-1}	$k_{pt\_release}$ s^{-1}
RFC$_{WT}$	1 ± 0.1	20 ± 0.6	2.7 ± 0.06
RFC-B$_{R84A}$	0.45 ± 0.1	19 ± 1.6	3.1 ± 0.1
RFC-C$_{R88A}$	0.8 ± 0.2	9 ± 0.7	0.8 ± 0.06
RFC-D$_{R101A}$	0.25 ± 0.1	16 ± 2	4.1 ± 0.4
RFC-BCD$_{AAA}$	< 0.1	4 ± 0.2	1.1 ± 0.3

Figure 3. Arginine mutants exhibit RFC subunit-specific defects in ptDNA binding, positioning, and release. *A*, ptDNA binding/positioning in RFC was measured by fluorescence increase on rapidly mixing ptDNA^{TAMRA} with RFC, PCNA, and non-hydrolyzable ATPγS (final concentrations: 0.1 μM RFC, 0.4 μM PCNA, 0.02 μM ptDNA^{TAMRA}, and 100 μM ATPγS). RFC-B^{R84A}, RFC-C^{R88A}, RFC-D^{R101A}, and RFC-BCD^{AAA} exhibit progressively slower rates compared with wild-type RFC; however, all achieve the same relative change in signal amplitude over time (except RFC-BCD^{AAA} reaches 75% in 60 s). *B*, a double mixing experiment, in which wild-type RFC and PCNA were first incubated with ATP with enough time for binding but not hydrolysis and then mixed with ptDNA^{TAMRA}, shows an initial signal decrease that depends on RFC concentration and yields a binding rate of 10^9 M^{-1} s^{-1} (*inset* shows a shorter time scale). A subsequent signal increase is independent of RFC concentration and yields a rate of 20 s^{-1}; the data were fit with a two-exponential function (final concentrations: 0.08, 0.1, and 0.15 μM RFC; 0.4 μM PCNA; 0.02 μM ptDNA^{TAMRA}; and 0.5 mM ATP). *C*, a double mixing experiment, in which RFC, PCNA, and ATP were first incubated with ptDNA^{TAMRA} for enough time to complete binding and then mixed with excess unlabeled ptDNA, shows signal increase at varying rates and extents with RFC mutants (*D*). A subsequent chase-dependent signal decrease reports ptDNA release at 2.7 ± 0.06 s^{-1} by wild-type RFC after ATP hydrolysis (supplemental Fig. S2C); the data were fit with a two-exponential function (final concentrations: 0.15 μM RFC, 0.4 μM PCNA, 0.02 μM ptDNA^{TAMRA}, 0.5 mM ATP, and 1 μM ptDNA). *D*, the table lists rates obtained from experiments in *B* and *C*. RFC-D^{R101A} binds ptDNA more slowly and appears to position only a small fraction compared with wild type, RFC-C^{R88A} positions and releases ptDNA more slowly than wild type, and RFC-BCD^{AAA} has very low activity overall.

ptDNA junction into a position that triggers ATP hydrolysis and completion of clamp loading. The arginine mutations perturb this ptDNA positioning step as well as described below.

Chase experiments were performed to monitor both isomerization and resolution of the initial collision complex through one catalytic turnover. In double mixing experiments, preformed RFC-ATP-PCNA$_{open}$ complex was mixed with ptDNA^{TAMRA} for 10 ms, which is just enough time to complete binding (Fig. 3*B*), followed by addition of excess unlabeled ptDNA to block rebinding of released ptDNA^{TAMRA}. As expected from the results in Fig. 3*B*, there is an increase in fluorescence as ptDNA is positioned within the clamp loader-open clamp complex (Fig. 3*C*). This phase is followed by a slow decay in fluorescence at 2.7 s^{-1}. Titration with unlabeled

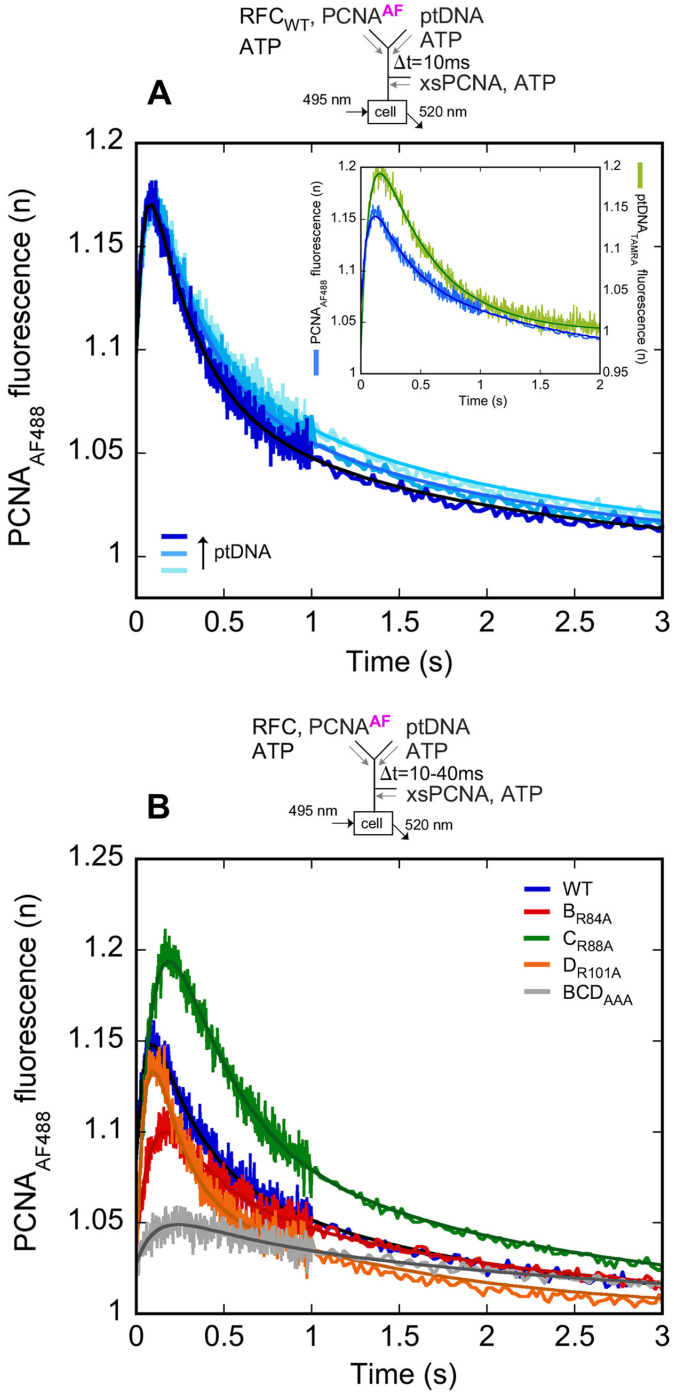

C

PCNA^{AF} transactions (ATP, ptDNA)	k_{P_open2} s^{-1}	k_{P_close} s^{-1}	$k_{P\_release}$ s^{-1}
RFC$_{WT}$	21 ± 1.5	4.4 ± 0.3	0.63 ± 0.03
RFC-B$_{R84A}$	10 ± 1.3	4.5 ± 0.8	0.53 ± 0.03
RFC-C$_{R88A}$	11 ± 0.4	2.7 ± 0.2	0.5 ± 0.02
RFC-D$_{R101A}$	19 ± 1.4	6.5 ± 0.6	0.7 ± 0.03
RFC-BCD$_{AAA}$	9 ± 1.7	2.3 ± 1.2	0.35 ± 0.04

Figure 4. Additional PCNA opening is induced by ptDNA binding/positioning in RFC. *A*, a double mixing experiment, in which wild-type RFC, PCNA^{AF}, and ATP (RFC-ATP-PCNA$_{open}$) were first incubated with ptDNA for enough time to complete binding and then mixed with excess unlabeled PCNA, shows initial ptDNA concentration-independent fluorescence increase at 21 s^{-1}, which reflects further PCNA opening. A subsequent signal decrease occurs in two phases: the first at 4.4 ± 0.3 s^{-1} is chase-independent and indicates PCNA closure (supplemental Fig. S3), and the second at 0.63 ± 0.03 s^{-1} is chase-dependent and indicates further PCNA closure upon release from RFC; the data were fit with a two-exponential function (final concentrations: 0.025 μM RFC; 0.02 μM PCNA^{AF}; 0.1, 0.2, and 0.4 μM ptDNA; 0.5 mM ATP; and 1 μM PCNA). The *inset* overlays PCNA^{AF} (*blue*) and ptDNA^{TAMRA} (*green*; Fig. 3*C*) traces, highlighting the coincidence of ptDNA positioning and secondary PCNA opening as well as ptDNA release and PCNA closure. *B*, in similar experiments with mutants, RFC-B^{R84A} and RFC-C^{R88A} exhibit slightly slower ptDNA-induced PCNA opening, whereas RFC-D^{R101A} is comparable with wild-type RFC; RFC-C^{R88A} also exhibits slower PCNA closure after ATP hydrolysis, resulting in complex accumulation; and RFC-BCD^{AAA} has very low activity overall. *C*, the table lists rates obtained from experiments in *A* and *B*.

ptDNA chase reveals that the signal decrease is due to release of ptDNA^{TAMRA} from RFC (supplemental Fig. S2C). As reported previously, ptDNA release occurs after ATP is hydrolyzed at a rate of 20–45 s^{-1} (17). The same experiment was performed with the mutants with the first mixing time varied from 10 to 40 ms to ensure maximal ptDNA binding in each case. RFC-B^{R84A} mutant appears similar to wild type with respect to ptDNA positioning and release rates, although a lower signal amplitude suggests that a smaller fraction of the isomerized complex is formed (Fig. 3, *C* and *D*). RFC-C^{R88A} exhibits slower ptDNA positioning, and the ~4-fold slower ptDNA release indicates disruption of subsequent steps in the reaction as well. RFC-D^{R101A} exhibits a much lower signal amplitude for ptDNA positioning, indicating that only a small fraction of the isomerized complex is formed, although the apparent rates of formation and decay are similar to those for wild-type RFC. RFC-BCD^{AAA} exhibits a combination of the defects seen with RFC-C^{R88A} and RFC-D^{R101A}; *i.e.* a small fraction of the complex forms slowly and decays slowly as well (Fig. 3, *C* and *D*). The results reveal a significant role for RFC-C Arg-88 and RFC-D Arg-101 in creating an activated RFC-ATP-PCNA$_{open}$-ptDNA complex that hydrolyzes ATP to complete clamp loading.

RFC-C Arg-88 promotes ptDNA-induced additional opening of PCNA and subsequent closure

The kinetic data thus far reveal that ptDNA is repositioned after binding to the RFC-ATP-PCNA$_{open}$ complex. We investigated what happens with PCNA during and after this step by analogous chase experiments measuring one catalytic turnover of the complex containing labeled PCNA^{AF} (this section) or PCNA^{MDCC} (next section). Preformed RFC-ATP-PCNA$^{AF}_{open}$ complex was mixed with ptDNA for 10 ms, which is just enough time to complete ptDNA binding (Fig. 3*B*), followed by addition of excess unlabeled PCNA to block rebinding of released PCNA^{AF}. To our surprise, there was an initial increase in Alexa Fluor 488 fluorescence, indicating further opening of PCNA at a rate of 21 s^{-1} (Fig. 4*A*). This rate is independent of ptDNA concentration, confirming that it reports an intramolecular event after DNA binds to the protein complex. A prior study of RFC ATPase mutants in which a FRET reporter assay was used to monitor PCNA opening also detected additional opening of the clamp after ptDNA binding (30). The similar kinetics of ptDNA positioning (20 s^{-1}) and ptDNA-induced secondary PCNA opening (21 s^{-1}) imply that these two events are coupled

in the reaction mechanism (Fig. 4*A*, *inset*) and together license ATP hydrolysis (20–45 s^{-1}; Ref. 17). The subsequent decay in signal, which reports PCNA closure, occurs in two phases (Fig. 4, *A* and *C*). The faster phase at 4.4 s^{-1} is independent of unlabeled PCNA chase (Fig. S3); therefore, we interpret that it reports an intramolecular event, *i.e.* PCNA closure while it remains bound to RFC. The rate is comparable with that of ptDNA release from RFC (2.7 s^{-1}; Fig. 3, *C* and *D*), implying that these two events are also coupled in the reaction mechanism. The second slower phase at 0.63 s^{-1} is dependent on unlabeled PCNA chase (supplemental Fig. S3); thus, it reports further clamp closure as PCNA-ptDNA complex dissociates from RFC. The rate is similar to the steady-state ATPase k_{cat} (0.8–1.2 s^{-1}; Refs. 15–17), indicating that release of PCNA from RFC after it closes around ptDNA may limit catalytic turnover.

The single mutants exhibit the same phenomenon of ptDNA-induced secondary PCNA opening with some interesting differences. With RFC-B^{R84A}, PCNA opens more slowly and to a lower fraction relative to wild type, but PCNA closure and release are comparable between the two (Fig. 4, *B* and *C*). Thus, it appears that ptDNA binding does not fully overcome the PCNA-opening defect in this mutant (Fig. 2*C*), but any activated RFC-ATP-$PCNA_{open}$-ptDNA complex that does form can complete PCNA loading at the same rate as wild-type RFC (Fig. 3, *C* and *D*). With RFC-C^{R88A}, PCNA opening is slower but so is closure; thus, the bound complex accumulates in the reaction (Fig. 4, *B* and *C*); this finding is in line with the slow release of $ptDNA^{TAMRA}$ (Fig. 3, *C* and *D*). With RFC-D^{R101A}, ptDNA appears to induce additional PCNA opening followed by closure and release with the same kinetics as wild-type RFC (Fig. 4, *B* and *C*). This finding is in sharp contrast to the lack of PCNA opening in the absence of ptDNA (Fig. 2*C*) and indicates that interaction with ptDNA relieves the clamp-opening defect in this mutant. It should also be noted that although RFC-D^{R101A} binds ptDNA, it is defective in positioning DNA within the complex (Fig. 3*C*). Together these results suggest that correct interaction with ptDNA has become uncoupled with secondary PCNA opening and completion of PCNA loading in this mutant. Finally, RFC-BCD^{AAA} exhibits very low activity, indicative of a combinatorial effect of the mutations.

RFC-C Arg-88 accelerates and RFC-D Arg-101 stalls ATP hydrolysis to coordinate efficient and selective loading of PCNA on ptDNA

As described in the previous section, monitoring a single turnover with labeled $PCNA^{AF}$ and $ptDNA^{TAMRA}$ revealed an unknown PCNA-opening step that is coincident with positioning of ptDNA and, importantly, appears to set up the complex for ATP hydrolysis. We explored the possibility of detecting other unknown steps by similar experiments with $PCNA^{MDCC}$, which reports interaction between RFC and PCNA (Fig. 2*A* and supplemental Fig. S1). Preformed RFC-ATP-$PCNA^{MDCC}{}_{open}$ complex was mixed with ptDNA for 10 ms, which is just enough time to complete DNA binding (Fig. 3*B*), followed by addition of excess unlabeled PCNA to block rebinding of released $PCNA^{MDCC}$ (Fig. 5*A*, *blue* trace). Indeed, there is further increase in $PCNA^{MDCC}$ fluorescence at ~8 s^{-1} that is independent of ptDNA concentration (supplemental Fig. S4A); thus, this reporter also reveals a conformational change in PCNA after ptDNA binding. Subsequent decrease in fluorescence occurs in two phases at 0.5 and 0.1 s^{-1}, both of which are dependent on PCNA chase and thus report dissociation-related events (supplemental Fig. S4B). The first decay rate is similar to that of clamp release after closing around ptDNA as reported by $PCNA^{AF}$ and is therefore interpreted as such (Fig. 4*A* and supplemental Fig. S3). The second decay is much slower than the steady-state ATPase rate (k_{cat} = 0.8–1.2 s^{-1}; Refs. 15–17), suggesting an off-pathway event. We detected a slow decrease in fluorescence simply by mixing $PCNA^{MDCC}$ with excess PCNA (data not shown); therefore, this phase appears to report slow subunit exchange between the labeled PCNA released from RFC and unlabeled chase. The single mutants also exhibit an increase in $PCNA^{MDCC}$ fluorescence that reports conformational change followed by signal decay that reports PCNA release after closure around ptDNA and then slow $PCNA^{MDCC}$-PCNA subunit exchange (Fig. 5*A*). RFC-C^{R88A} shows the most striking difference compared with wild-type RFC with slower change in PCNA conformation and release that results in complex accumulation as reported by $ptDNA^{TAMRA}$ (Fig. 3*C*) and $PCNA^{AF}$ (Fig. 4*B*) as well. RFC-B^{R84A} and RFC-D^{R101A} kinetics appear more similar to wild-type RFC, although a lower signal suggests a smaller fraction of complex or some difference in conformation. RFC-BCD^{AAA} shows no increase in $PCNA^{MDCC}$ fluorescence, only slow decay.

A 1-s overlay of $PCNA^{MDCC}$ (Fig. 5*A*) and $ptDNA^{TAMRA}$ (Fig. 3*D*) traces with wild-type RFC shows that the conformational change reported by $PCNA^{MDCC}$ occurs after positioning of ptDNA in the complex (Fig. 5*B*). We also compared the timing of these events with ATP hydrolysis and phosphate (P_i) release measured under pre-steady-state conditions. As reported previously (17), wild-type RFC and PCNA were premixed with [^{32}P]ATP or ATP for 3 s to complete ptDNA-independent clamp opening and then mixed with ptDNA to measure [^{32}P]ADP formation or with MDCC-labeled phosphate-binding protein (PBP^{MDCC}) to measure P_i release. ptDNA triggers a rapid burst of ATP hydrolysis (30 s^{-1}) and P_i release (~8 s^{-1}) followed by a linear steady-state phase at k_{cat} = 1 s^{-1} (Fig. 5*B*); in the absence of ptDNA, there is no burst, and k_{cat} = 0.06 s^{-1} (Fig. 5*C* and supplemental Fig. S5). A visual comparison in Fig. 5*B* indicates that the conformational change reported by the increase in $PCNA^{MDCC}$ fluorescence occurs in the lag period between ATP hydrolysis and P_i release. As described under "Discussion," the timing of events in the reaction was resolved by fitting all the wild-type RFC data simultaneously to develop a model for the clamp-loading mechanism (Scheme 1 and Fig. 6). Like wild-type RFC, the mutants do not exhibit any burst of P_i release in the absence of ptDNA with or without PCNA (Fig. 5*C* and supplemental Fig. S5; note that in the absence of ptDNA RFC-D^{R101A} k_{cat} is significantly faster than that of wild-type RFC). When mixed with ptDNA, RFC-B^{R84A} exhibits a full burst of P_i release, which indicates that any PCNA-opening and ptDNA-binding defects in this mutant are relatively minor and do not disrupt the critical ATP hydrolysis step in the reaction. With RFC-C^{R88A}, the burst of P_i release is suppressed, which indicates that the ptDNA positioning and

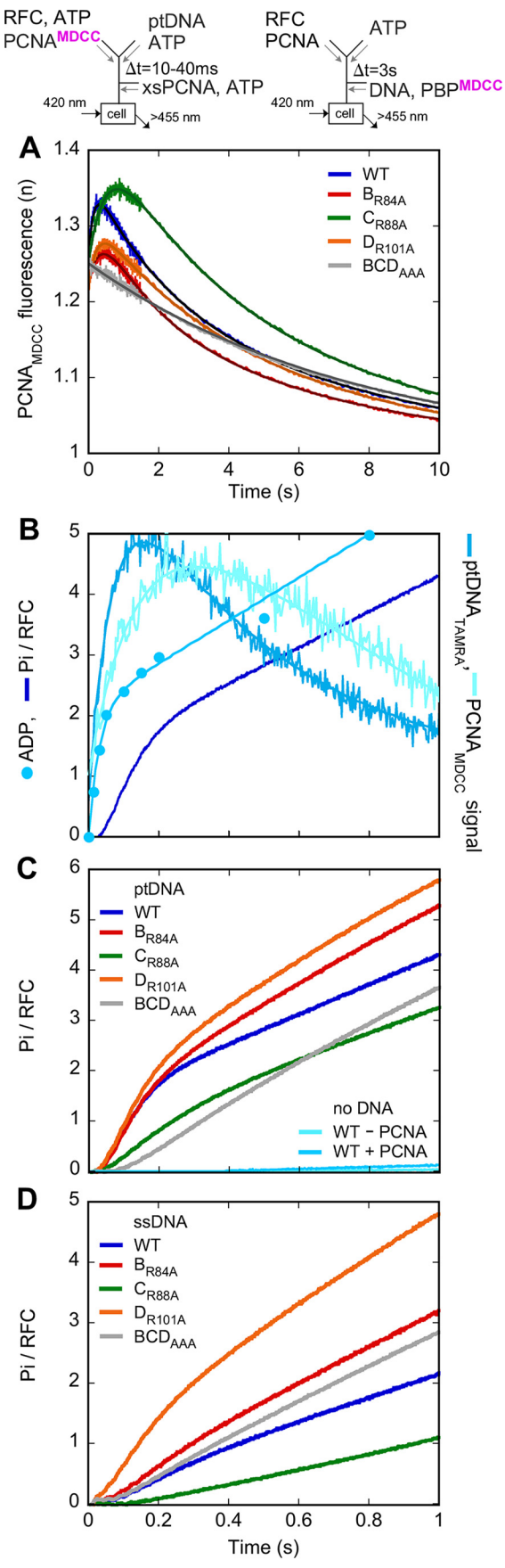

Figure 5. RFC-C Arg-88 enables completion of PCNA loading on binding of ptDNA, and RFC-D Arg-101 confers specificity for ptDNA. *A*, a double mixing experiment, in which RFC, $PCNA^{MDCC}$, and ATP (RFC-ATP-$PCNA_{open}$) were first incubated with ptDNA for enough time to complete binding and then mixed with excess unlabeled PCNA, shows initial fluorescence increase at ~8 s^{-1}. The rate is independent of ptDNA concentration (supplemental Fig. S4A), indicating PCNA isomerization. Subsequent chase-dependent signal decrease occurs in two phases (supplemental Fig. S4B): at 0.5 ± 0.02 s^{-1}, reflecting PCNA release from RFC, and at 0.1 ± 0.003 s^{-1}, likely due to $PCNA^{MDCC}$ subunit exchange with unlabeled PCNA; the data were fit with a three-exponential function (final concentrations: 0.025 μM RFC, 0.02 μM $PCNA^{MDCC}$, 0.15 μM ptDNA, 0.5 mM ATP, and 1 μM PCNA). RFC-C^{R88A} exhibits slower PCNA isomerization and release compared with wild-type RFC, and RFC-BCD^{AAA} exhibits no PCNA isomerization, only slow release. *B*, an overlay of wild-type RFC kinetics after formation of the RFC-ATP-$PCNA_{open}$-ptDNA collision complex allows visual comparison of rapid ptDNA positioning at 20 s^{-1} ($ptDNA^{TAMRA}$ signal increase; Fig. 3*C*), a burst of ATP hydrolysis at 30 ± 5 s^{-1} ([^{32}P]ADP formation reported previously (17)), PCNA isomerization ($PCNA^{MDCC}$ signal increase; *A*), P_i release after a slight lag (PBP^{MDCC} signal increase; *C*), and PCNA release ($PCNA^{MDCC}$ signal decrease; *A*). *C*, double mixing experiments, in which RFC and PCNA were first incubated with ATP for enough time to open PCNA and then mixed with ptDNA and PBP^{MDCC} reporter, show a burst of P_i release in the first turnover followed by a linear steady state for wild-type RFC, RFC-B^{R84A}, and RFC-D^{R101A}. RFC-C^{R88A} shows almost no burst, and RFC-BCD^{AAA} shows a lag (final concentrations: 0.5 μM RFC, 1 μM PCNA, 2.5 μM ptDNA, 0.5 mM ATP, and 10 μM PBP^{MDCC}). ATPase activity of wild-type RFC in the absence of DNA (± PCNA) is also shown. *D*, in analogous experiments with ssDNA, only RFC-D^{R101A} exhibits a burst of P_i release comparable with that of wild-type RFC with ptDNA (*C*).

secondary PCNA-opening defects in this mutant disrupt ATP hydrolysis and completion of clamp loading. RFC-D^{R101A} exhibits a full burst of P_i release, which is surprising given $ptDNA^{TAMRA}$ data showing that this mutant has a severe defect in positioning DNA within the complex (Fig. 3*C*). However, the $PCNA^{AF}$ data showed that RFC-D^{R101A} has no defect in ptDNA-induced secondary clamp opening (Fig. 4*B*). As noted earlier, together these results indicate that RFC-D^{R101A} does not require proper interaction with ptDNA to go forward with the clamp-loading reaction. Finally, like RFC-C^{R88A}, the triple mutant RFC-BCD^{AAA} exhibits no burst activity, confirming the overriding importance of RFC-C Arg-88 for accelerating ATP hydrolysis.

The intriguing finding that RFC-D^{R101A} is insensitive to correct positioning of ptDNA within the RFC-ATP-$PCNA_{open}$ complex suggested that this mutation relaxes RFC selectivity for ptDNA as the substrate for loading PCNA. We tested this hypothesis by measuring P_i release in the presence of single-stranded DNA instead of ptDNA. ssDNA binding stimulates wild-type RFC ATPase activity but does not trigger a significant burst of ATP hydrolysis and P_i release (Fig. 5*D* and supplemental Fig. S5; k_{cat} = 0.3 s^{-1}), confirming that the latter response is specific to ptDNA and enables selective loading of PCNA on this DNA substrate. When mixed with ssDNA, RFC-B^{R84A}, RFC-C^{R88A}, and RFC-BCD^{AAA} show ATPase profiles similar to that of wild-type RFC (no/low burst activity). RFC-D^{R101A}, however, exhibits a promiscuous burst of ATP hydrolysis, which confirms a critical role for the RFC-D Arg-101 residue in selecting ptDNA as the correct substrate for loading PCNA.

Discussion

A clamp loader brings together two substrates, a clamp and ptDNA; opens the clamp and positions ptDNA within; enables clamp closure around ptDNA; and releases the topologically linked clamp-ptDNA product in a catalytic reaction driven by a third substrate, ATP. The focus of this study was on the coordination between all moving parts that constitute the clamp-

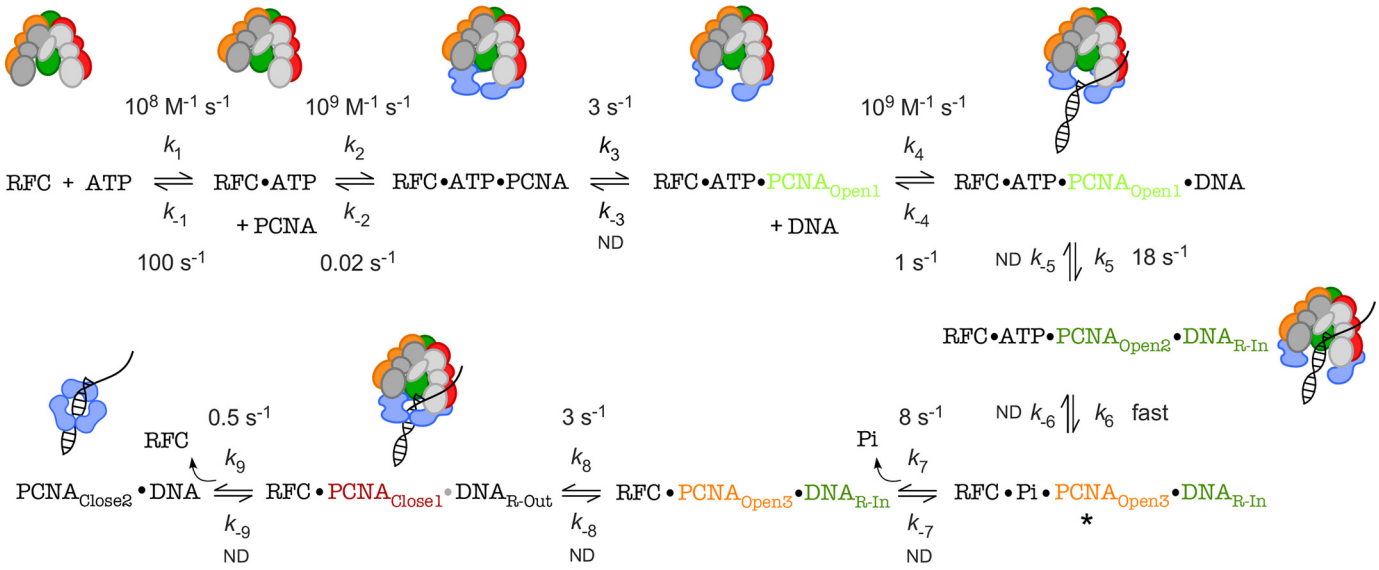

Scheme 1. A kinetic model of the RFC-catalyzed PCNA-loading mechanism. All experimental data for wild-type RFC were fit to this model with measured rate constants used as initial estimates for global fitting (Fig. 6). Key conformational changes reported by PCNA and ptDNA are highlighted by *subscript labels*. $PCNA_{Open1}$ is in a partially open state before and after initial contact with ptDNA ($DNA_{R\text{-}On}$). $PCNA_{Open2}$ is in a fully open state as ptDNA is positioned in the complex ($DNA_{R\text{-}In}$). $PCNA_{Open3}$ is a state after ATP hydrolysis but before clamp closure. $PCNA_{Close1}$ denotes clamp closure as ptDNA is released from RFC ($DNA_{R\text{-}Out}$). $PCNA_{Close2}$ is a final closed state loaded on ptDNA. * indicates that $PCNA_{Open3}$ may occur with step 7 (P_i release). Rate constants obtained from global analysis of the data are noted at each step. *ND*, not determined.

loading reaction. The specific goals were to (*a*) refine our current understanding of the kinetic mechanism (15, 16) by monitoring transient events in one catalytic turnover reported by all three substrates and (*b*) address an intriguing hypothesis that implicates a DNA-binding residue in ATP hydrolysis (3, 13) by analyzing the effects of its mutation to alanine. The results revealed two new steps in the mechanism: a concerted adjustment of both PCNA and ptDNA after binding to RFC that green-lights ATP hydrolysis and another adjustment upon ATP hydrolysis that signals PCNA closure and PCNA-ptDNA release (Scheme 1, steps 5 and 6). The existence of these two steps, akin to checkpoints completing the assembly and initiating the disassembly stages of the reaction, respectively, had been inferred from our previous studies of RFC (15, 16); here the nature of these steps is resolved. The kinetic analysis also revealed that the DNA-binding residue in question is a linchpin in the mechanism as it links RFC transactions with all three substrates and at all steps of the reaction.

A model for RFC-catalyzed PCNA loading with key transitions between assembly and disassembly stages of the reaction

All of the kinetic data obtained for wild-type RFC in this study were fit simultaneously to various models of the clamp-loading mechanism using KinTek Explorer (42) with a previously published version as the starting point (15, 16). The goal was to revise the earlier model as directed by new data from experiments with labeled $PCNA^{MDCC}$, $PCNA^{AF}$, and $ptDNA^{TAMRA}$ reporting one turnover of the reaction. The measured rates were used as initial estimates for global fitting. The best-fit model and the rates obtained from it are shown in Scheme 1, and the fits are shown with corresponding experimental data in Fig. 6. A description of the model is provided below, relating the transient events to available clamp and clamp loader structures. The reaction begins with ATP binding to RFC fixed at $k_1 = 1 \times 10^8$ M^{-1} s^{-1} and $k_{-1} = 100$ s^{-1} (we assumed rapid binding because the kinetics are independent of ATP concentration in our experiments and set the K_D to 1 μM as reported previously for ATPγS; Refs. 17 and 30). PCNA binds to ATP-bound RFC with $k_2 = 1.1 \pm 0.04 \times 10^9$ M^{-1} s^{-1} and $k_{-2} = 0.022$ s^{-1} (the K_D was set to 0.02 nM as measured; Fig. 2*A* and supplemental Fig. S1). RFC binds PCNA rapidly in the absence of ATP, but this complex dissociates ~1500-fold faster than the ATP-bound complex (supplemental Fig. S1); hence, we did not include a path without ATP in the model. PCNA opening occurs next, relatively slowly at $k_3 = 3.1 \pm 0.1$ s^{-1}, consistent with the previously reported rate (16, 39, 40); allowing k_{-3} to float during data fitting yielded a low value; hence, it was set to zero. The AAA+ modules in ATP-bound clamp loader structures adopt a right-handed spiral conformation that complements an open clamp (3, 12, 31). In the *S. cerevisiae* RFC-ATPγS-PCNA structure, PCNA is in a closed planar form in contact with the lower arm of the RFC spiral (Fig. 1*B* and Ref. 12) and can adopt an open form in contact with both arms (Fig. 1*C* and Ref. 35). We have reported previously that RFC-PCNA interaction drives additional ATP binding to RFC, promoting its activation and PCNA opening (17, 30). In this context, the RFC-ATPγS-PCNA structure likely reflects an early complex formed in step 2 of the model, and coupled conformational changes in both proteins slowly stabilize the twisted open form in step 3 (Scheme 1). Such a two-step clamp-opening mechanism has been proposed for both *E. coli* and *S. cerevisiae* proteins (22, 39).

Next, ptDNA binds to the RFC-ATP-$PCNA_{Open1}$ complex at $k_4 = 1 \pm 0.04 \times 10^9$ M^{-1} s^{-1} and $k_{-4} = 1$ s^{-1} (the K_D was set to 1 nM as reported previously (15)). RFC can also bind ptDNA-absent PCNA, but this complex takes longer to form and is less stable (15, 17); because all DNA-binding experiments were con-

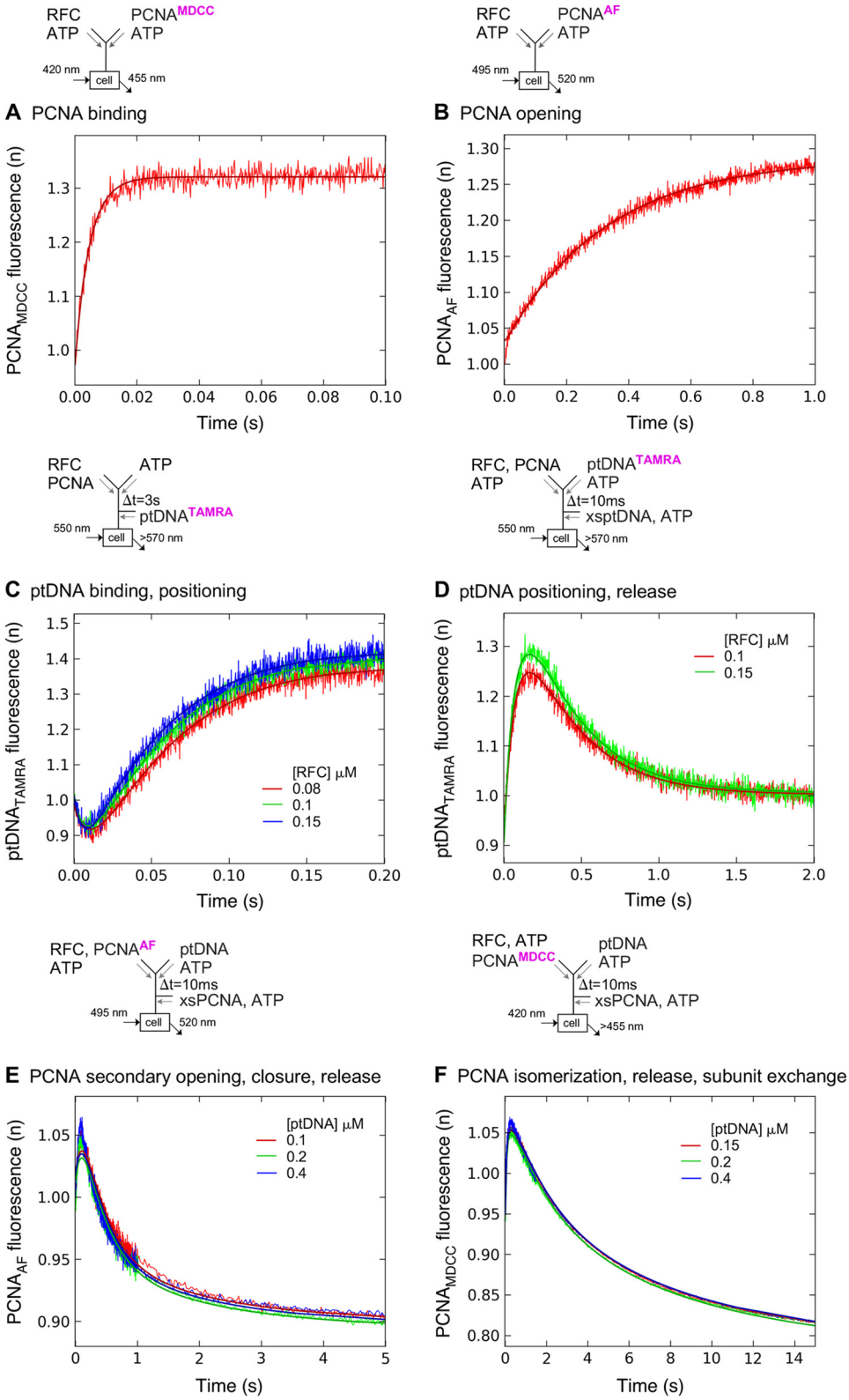

Figure 6. Global fitting of kinetic data to an RFC-catalyzed PCNA-loading mechanism. All kinetic data for wild-type RFC were fit simultaneously using KinTek Explorer (42) to the model shown in Scheme 1. The *smooth lines* overlaid on the data are fits generated by the model based on the kinetic parameters noted in Scheme 1. *A*, PCNA binding to RFC measured by increase in $PCNA^{MDCC}$ fluorescence. *B*, PCNA opening by RFC measured by increase in $PCNA^{AF}$ fluorescence. *C*, DNA binding and positioning measured by decrease and increase in $ptDNA^{TAMRA}$ fluorescence, respectively. *D*, DNA positioning followed by release after ATP hydrolysis measured by increase and decrease in $ptDNA^{TAMRA}$ fluorescence, respectively. *E*, additional PCNA opening followed by closure and release after ATP hydrolysis measured by increase and decrease in $PCNA^{AF}$ fluorescence, respectively. *F*, PCNA isomerization and release after ATP hydrolysis (followed by subunit exchange with unlabeled PCNA) measured by increase and decrease in $PCNA^{MDCC}$ fluorescence, respectively.

ducted with PCNA-bound RFC, for simplicity we did not include a path lacking PCNA in the model. After formation of the RFC-ATP-$PCNA_{Open1}$-ptDNA collision complex in step 4, a new step was introduced into the model involving adjustment of the ptDNA position coincident with additional PCNA opening at $k_5 = 17 \pm 0.5\ s^{-1}$ (reported by $ptDNA^{TAMRA}$ (Fig. 3*B*) and $PCNA^{AF}$ (Fig. 4*A*), respectively); allowing k_{-5} to float during data fitting yielded a low value; hence, it was set to zero. After ptDNA binding, RFC catalyzes a burst of ATP hydrolysis at $30\ s^{-1}$ (Fig. 5*B*). The similarity between the two rates suggests that k_5 limits the observed rate of ATP hydrolysis. Indeed, the model yields an unrestrained fast rate for hydrolysis of 3 ± 0.2 ATP molecules ($k_6 > 1000\ s^{-1}$) after the conformational change in step 5 creates the RFC-ATP-$PCNA_{Open2}$-$ptDNA_{R\text{-}In}$ complex. The AAA+ modules in ptDNA-bound clamp loader structures are tightly packed around the duplex portion such that the ATPase sites are in a catalytically active state (13, 31). Notably, the T4 and *Pyrococcus furiosus* complex structures show clamp and clamp loader openings that are too narrow for direct entry of dsDNA (13, 43), and it has been proposed that the single-stranded template enters first followed by upward movement of the duplex until the primer end abuts the top of the chamber and the template exits through a gap (3). Step 5 described above fits the bill for isomerization of the initial binding complex. Importantly, this slow step could verify the correct ptDNA substrate right before stimulation of ATP hydrolysis. We have shown previously that ssDNA alone binds and dissociates rapidly from the RFC-ATP-PCNA complex without triggering a burst of ATP hydrolysis (15, 41). Conversely, a short duplex with free ends can slide up through the bottom of the complex and trigger a full burst of ATP hydrolysis (supplemental Fig. S5). A two-step "enter and slide up" binding mechanism would increase specificity for DNA structures containing both single- and double-stranded segments. A recent small-angle X-ray scattering analysis of *E. coli* γ complex-β indicates that the clamp can open more widely in solution than observed in crystal structures (44). This finding is consistent with our data showing secondary PCNA opening in step 5 as ptDNA moves inside the complex to complete the assembly stage of the reaction.

Another new step was introduced next into the model involving a conformational change in PCNA (reported by $PCNA^{MDCC}$; Fig. 5*A*). We tested alternative models in which this step occurred before, with, or after ATP hydrolysis. The best global fit was obtained when PCNA isomerization was either coincident with ATP hydrolysis ($k_6 > 1000\ s^{-1}$) followed by slow P_i release ($k_7 = 8.2 \pm 0.2\ s^{-1}$) or after hydrolysis and coincident with P_i release but not if it occurred before ATP hydrolysis; allowing k_{-7} to float during data fitting yielded a low value; hence, it was set to zero. The kinetics of ADP release from RFC have not been measured yet; hence, it was not included explicitly in the model; the presence of ADP in a T4 gp44/62 structure suggests it is stably bound and likely released slower than P_i (13). Step 8 in the model is ptDNA release from RFC coincident with closure of PCNA at $k_8 = 2.9 \pm 0.04\ s^{-1}$; allowing k_{-8} to float during data fitting yielded a low value; hence, it was set to zero. In the earlier version of the model, PCNA closure was associated with P_i release (step 7), consistent with the slightly faster measured rate of $8\ s^{-1}$; differences in the assay and/or absence of unlabeled chase in previous experiments may explain the variation (15, 16). Step 8 yields RFC-ATP-$PCNA_{Close1}$-$ptDNA_{R\text{-}Out}$ complex, reflecting the fact that despite loss of contact between ptDNA and RFC the disassembly process is not complete. The short $ptDNA^{TAMRA}$ with free ends in our experiments slips out of the complex into solution and is lost amid excess unlabeled ptDNA (supplemental Fig. S2*C*); however, *in vivo*, ptDNA would be handed off from RFC to PCNA as the clamp closes around it. The last step in the model is PCNA release from RFC (reported by $PCNA^{MDCC}$; supplemental Fig. S4) coincident with its adjustment into a final closed form around ptDNA (reported by $PCNA^{AF}$; supplemental Fig. S3) at $k_9 = 0.55 \pm 0.02\ s^{-1}$; allowing k_{-9} to float during data fitting yielded a low value; hence, it was set to zero. It has been proposed previously that a two-step "closure and release" mechanism would minimize the possibility of complex disassembly before the clamp closes around DNA (18).

A T4 gp44/62-gp45 structure with one ADP-bound subunit sheds light on how ATP hydrolysis could complete complex disassembly (13). The ADP-bound AAA+ module is in a conformation that breaks the spiral symmetry of the clamp loader. Moreover, the nucleotide-free structure of *E. coli* γ complex does not form a spiral (11). Thus, it has been proposed that a cascade of ATP hydrolysis along the clamp loader subunits disrupts their spiral configuration, weakening their contacts with ptDNA and the clamp. The single burst of three ATP molecules hydrolyzed per turnover measured for RFC (Fig. 5*C* and Refs. 15 and 17) and *E. coli* γ complex (20, 45) indicates a concerted reaction, but a sequential mechanism could also be consistent with the data if there were no intervening slow step between each ATP hydrolysis. In this context, PCNA isomerization coincident with ATP hydrolysis (step 6) or P_i release (step 7) likely reflects a change in PCNA interaction with RFC that is a harbinger of its coming full break from the clamp loader (step 9). Mutations of PCNA inner rim residues that bind ptDNA slow down closure (16), suggesting that as ptDNA is handed off from RFC to PCNA (step 8) closer contact between the two substrates and tilting of the PCNA clamp on ptDNA (7, 9) facilitate its release from RFC.

RFC-DNA contacts allosterically mediate key transitions in the reaction

The kinetic mechanism described above illustrates the links between RFC transactions with PCNA, ptDNA, and ATP. The detailed information enables specific testing of hypotheses about these links, and in this study, we focused on a DNA-binding residue that is proposed to regulate ATP hydrolysis and lies in a loop preceding a clamp-binding α helix (3, 12). The arginine is one of three conserved basic residues in each RFC subunit that interact with DNA, and this particular one is thought to bind Walker B glutamate in the absence of DNA and turn it catalytically "off" for ATP hydrolysis or release glutamate upon binding DNA and turn it "on" instead. This switch hypothesis predicts that removal of the arginine would lift the hold on ATP hydrolysis and thus accelerate ATPase activity even in the absence of DNA. To test this hypothesis, we mutated arginine to alanine individually and together in RFC-B

(Arg-84), RFC-C (Arg-88), and RFC-D (Arg-101) subunits. In the absence of ptDNA, none of the mutants exhibited a burst of ATP hydrolysis that is the hallmark of ptDNA-bound RFC (~500-fold increase from a basal rate of 0.06 to ~30 s^{-1}; Fig. 5*B* and supplemental Fig. S5); thus, the switch hypothesis did not hold. We noted that loss of Arg-101 in the RFC-D subunit did lead to a slight increase in the ATPase rate (~5-fold), indicating more subtle subunit-specific effects at play (supplemental Fig. S5). The presence of ptDNA stimulated burst ATPase activity in RFC-B^{R84A} and RFC-D^{R101A} mutants, which initially suggested that RFC-B Arg-84 and RFC-D Arg-101 do not have a significant role in ptDNA binding and positioning and subsequent steps in the reaction. In contrast, ptDNA was unable to stimulate a burst in RFC-C^{R88A}, which indicated that contact between RFC-C Arg-88 and ptDNA is in fact necessary to accelerate ATP hydrolysis (Fig. 5*C*). The lack of a burst in the triple RFC-BCD^{AAA} mutant confirms the predominant role of RFC-C subunit in stimulating ATPase activity. Subsequent kinetic analysis with $ptDNA^{TAMRA}$, $PCNA^{MDCC}$, and $PCNA^{AF}$ clarified the distinct contributions of each arginine to the PCNA-loading mechanism.

The results with $ptDNA^{TAMRA}$ show that loss of even one residue in the extensive DNA-binding interface presented by RFC can alter the interaction. The effects vary by subunit: loss of RFC-D Arg-101 results in less ptDNA correctly positioned with the junction at the top of the RFC chamber, and loss of RFC-C Arg-88 slows down ptDNA positioning, whereas loss of RFC-B Arg-84 has a relatively small effect (Fig. 3*C*). These outcomes could be due to direct disruption of RFC interaction with DNA and/or indirect effects via perturbation of the Walker B glutamate (28) that in turn disrupt ATP-induced ptDNA binding or PCNA opening-coupled ptDNA positioning (Fig. 4). We tested these possibilities in experiments with $PCNA^{MDCC}$ and $PCNA^{AF}$. The results showed that ATP increases the affinity of all mutants for PCNA overall, but they are defective in PCNA opening with the most disruption caused by loss of RFC-D Arg-101 > RFC-C Arg-88 > RFC-B Arg-84 (Fig. 2*C*). We have previously proposed that the central RFC-*C* subunit serves as a pivot for twisting open the arms of the PCNA spiral (30). Here we propose that RFC-D serves as an anchor for the upper arm of the open PCNA spiral, an interpretation that is consistent with the structures of closed and open PCNA-bound RFC (Fig. 1 and Refs. 12 and 35). Notably, the disruptive effects of mutating an arginine that contacts ptDNA on ptDNA-independent, ATP-induced PCNA opening confirm the central role of this residue in RFC transactions with all three substrates.

ptDNA induces additional opening of PCNA by all single mutants to varying extents. Loss of RFC-B Arg-84 slows down this secondary PCNA opening (Fig. 4, *B* and *C*), but ptDNA positioning is relatively unaffected (Fig. 3*C*), and the resulting complex proceeds through a burst of rapid ATP hydrolysis and P_i release (Fig. 5*C*), PCNA closure (Fig. 4, *B* and *C*), ptDNA release (Fig. 3*C*), and disassembly (Fig. 5*A*) at rates comparable with wild-type RFC. These findings are consistent with a prior study in which inactivation of the RFC-B ATPase site had just a moderate impact on the reaction (30). Loss of RFC-C Arg-88 also slows down secondary PCNA opening (Fig. 4, *B* and *C*), but in this case, ptDNA positioning is also slow (Fig. 3, *C* and *D*), which explains the lack of an ATPase burst (Fig. 5*C*), subsequent slow ptDNA release (Fig. 3, *C* and *D*), and PCNA closure (Fig. 4, *B* and *C*), leading to accumulation of ATP- and ptDNA-bound open-clamp intermediate(s). These findings confirm that contact between the Arg-88 residue in RFC-C and ptDNA serves to accelerate completion of PCNA loading after the complex is fully assembled. The predominant role of RFC-C in productive ptDNA binding was noted in an earlier study of ATPase-inactive RFC mutants as well (30). Loss of RFC-D Arg-101 has no effect on the secondary PCNA opening rate (Fig. 4, *B* and *C*). This result is surprising because the mutation has a significant disruptive effect on the positioning of ptDNA (Fig. 3*C*), which is tightly coupled to PCNA opening in wild-type RFC. More startling is the full burst of ATP hydrolysis (Fig. 5*C*) followed by PCNA closure and release at rates comparable with wild-type RFC (Fig. 4, *B* and *C*), suggesting that correct interaction with ptDNA is uncoupled from completion of clamp loading in this mutant. This hypothesis was tested by measuring the effect of an incorrect substrate, ssDNA, on ATP hydrolysis. Indeed, ssDNA triggers a burst of ATP hydrolysis by RFC-D^{R101A} but not by wild-type RFC, RFC-B^{R84A}, RFC-C^{R88A}, or RFC-BCD^{AAA}. This result indicates that RFC-B and RFC-C are not capable of discriminating between ssDNA and ptDNA and confirms that the Arg-101 residue in RFC-D serves as a brake on PCNA loading until it specifically contacts ptDNA. In this role, Arg-101 does act as a specialized "master switch," inhibiting ATP hydrolysis until it can interact with the correct DNA substrate. Notably, RFC-D is the final ATPase-active subunit to contact ptDNA as it winds up the RFC chamber with Arg-101 being the last of the three Walker B glutamate-binding arginines to interact with the template backbone (supplemental Fig. S6) (12, 13, 31). This location underlies the utility of its hold on ATP hydrolysis by all three subunits, which is released once ptDNA is fully in position.

In conclusion, the results of this study have further elucidated the clamp-loading mechanism and revealed new information on how individual clamp loader subunits contribute in discrete but coordinated ways toward efficient loading of clamps onto ptDNA based on their location in the complex. The findings will inform future structure–function analysis of clamp loaders and other members of the large AAA+ protein family.

Experimental procedures

Buffers

All experiments, unless noted otherwise, were performed in Buffer A containing 30 mM Hepes-NaOH (pH 7.5), 100 mM NaCl, 10 mM $MgCl_2$, 2 mM DTT. RFC was stored in 30 mM Hepes-NaOH (pH 7.5), 250 mM NaCl, 0.5 mM EDTA, 5% glycerol. PCNA was stored in 30 mM Hepes-NaOH (pH 7.5), 20 mM NaCl, 5% glycerol. All assays were performed at 25 °C.

DNA, protein, and other reagents

ATP and ATPγS were purchased from Sigma-Aldrich. MDCC, Alexa Fluor 488, and TAMRA dyes were obtained from Thermo Fisher. DNAs were purchased from Integrated DNA Technologies and purified by urea gel electrophoresis. ptDNA was prepared by annealing 40-nt primer (5′-ATT TCC TTC

AGC AGA TAG GAA CCA TAC TGA TTC ACA TGG C-3′) and 65-nt template (5′-TAG TTA GAA CCT AAG CAT ATT AGT AGC CAT GTG AAT CAG TAT GGT TCC TAT CTG CTG AAG GAA AT-3′); dsDNA was prepared by annealing the 40-nt primer to its complement. TAMRA-labeled 40-nt primer was prepared by labeling the 3′-end modified with an amino linker as described previously (17). Primers used for the mutagenesis of RFC were: 5′-GAA CGC TTC AGA TGA CGC AGG TAT TGA TGT CGT C-3′ (RFC-B^{R84A}, forward), 5′-GAC GAC ATC AAT ACC TGC GTC ATC TGA AGC GTT C-3′ (RFC-B^{R84A}, reverse), 5′-CAC TGC ATC CGA TGA CGC AGG TAT TGA TGT GTT G-3′ (RFC-C^{R88A}, forward), 5′-CAC CAC ATC AAT ACC TGC GTC ATC GGA TGC ATT C-3′ (RFC-C^{R88A}, reverse), 5′-GTT GAA CGC TTC TGA CGA AGC TGG TAT CTC TAT TGT AAG AG-3′ (RFC-D^{R101A}, forward), and 5′-CTC TTA CAA TAG AGA TAC CAG CTT CGT CAG AAG CGT TCA AC-3′ (RFC-B^{DR101A}, reverse). Wild-type and mutant *S. cerevisiae* RFC proteins were expressed in *E. coli* BL21(DE3) cells using a dual vector system with full-length RFC-A/E on pLANT2 and RFC-B/C/D on pET11a and purified as described (46). Point mutations to generate RFC-B^{R84A}, RFC-C^{R88A}, and RFC-D^{R101A} were made in pET11a-RFC-B/C/D by site-directed mutagenesis (QuikChange kit, Agilent Technologies). Coexpression of pET11a-RFC-B^{R84A}/C/D, pET11a-RFC-B/C^{R88A}/D, or pET11a-RFC-B/C/D^{R101A} with pLANT2-RFC-A/E yielded RFC complexes with Arg mutated to Ala in individual subunits. Coexpression of pET11a-RFC-B^{R84A}/C^{R88A}/D^{R101A} with pLANT2-RFC-A/E yielded the RFC triple mutant. Wild-type PCNA, $PCNA^{I111C/I181C}$ (C22S/C62S/C81S/I111C/I181C; from Linda Bloom, University of Florida) and $PCNA^{S43C}$ (C22S/C62S/C81S/S43C; from Linda Bloom, University of Florida) were expressed in BL21(DE3) cells and purified as described (15). $PCNA^{I111C/I181C}$ was labeled with Alexa Fluor 488 ($PCNA^{AF}$) and $PCNA^{S43C}$ was labeled with MDCC ($PCNA^{MDCC}$) as described (39). *E. coli* PBP was purified and labeled with MDCC as described (47). Protein concentrations were determined by Coomassie Plus assay (Pierce).

PCNA binding and release

PCNA binding to RFC was measured by monitoring $PCNA^{MDCC}$ fluorescence (λ_{ex} = 420 nm, λ_{em} > 450 nm) on a stopped-flow instrument (KinTek Corp., Austin, TX) using a single mixing scheme in which wild-type or mutant RFC (±ATP) was mixed with $PCNA^{MDCC}$ (±ATP) (final concentrations: 0.1, 0.2, and 0.4 μM RFC; 0.02 μM $PCNA^{MDCC}$; and 0.5 mM ATP). The signal from four to six traces was averaged for each experiment, normalized to initial value, and fit to a single-exponential function to determine the binding rate, k, and the bimolecular binding rate constant, $k_{on} = k/[RFC]$ (k_2 in the model). All reported data are from two to three independent experiments, and the standard error of the fit is provided. PCNA dissociation from RFC was measured by mixing RFC and $PCNA^{MDCC}$ (±ATP) with unlabeled PCNA chase (±ATP) (final concentrations: 0.2 μM RFC, 0.02 μM $PCNA^{MDCC}$, 0.5 mM ATP, and 1 μM PCNA). The signal from four to six traces was averaged for each experiment, normalized to final value, and fit to a single-exponential function to determine the dissociation rate, k_{off} (k_{-2} in the model). PCNA release from RFC after ptDNA binding, ATP hydrolysis, and ring closure was measured by monitoring $PCNA^{MDCC}$ fluorescence on a stopped-flow instrument using a double mixing scheme. RFC, $PCNA^{MDCC}$, and ATP were first mixed with ptDNA and ATP (Δt = 10 ms for RFC and RFC-B^{R84A}, Δt = 15 ms for RFC-C^{R88A}, Δt = 20 ms for RFC-D^{R101A}, and Δt = 40 ms for RFC-BCD^{AAA} to complete ptDNA binding) followed by mixing with unlabeled PCNA chase and ATP (final concentrations: 0.025 μM RFC, 0.02 μM $PCNA^{MDCC}$, 0.15 μM ptDNA, 0.5 mM ATP, and 1 μM PCNA). The signal from four to six traces was averaged for each experiment, normalized to final value, and fit to a three-exponential function to determine PCNA isomerization and release rates (k_6 and k_9, respectively, in the model); the third rate was slower than the steady-state rate of the reaction and was found to be an off-pathway decrease in $PCNA^{MDCC}$ signal due to slow subunit exchange with excess unlabeled PCNA.

PCNA opening and closure

PCNA opening was measured by monitoring $PCNA^{AF}$ fluorescence (λ_{ex} = 495 nm, λ_{em} = 520 ± 10 nm) on a stopped-flow instrument using a single mixing scheme in which RFC (±nucleotide) was mixed with $PCNA^{AF}$ (±nucleotide) (final concentrations: 0.2 μM RFC, 0.02 μM $PCNA^{AF}$, and 0.5 mM ADP or ATP). The signal from four to six traces was averaged for each experiment, normalized to initial value, and fit to a single-exponential function to determine the opening rate (k_3 in the model). PCNA closure after ptDNA binding and ATP hydrolysis was measured by monitoring $PCNA^{AF}$ fluorescence on a stopped-flow instrument using a double mixing scheme. RFC, $PCNA^{AF}$, and ATP were first mixed with ptDNA and ATP (Δt = 10 ms to allow ptDNA binding) followed by mixing with unlabeled PCNA chase and ATP (final concentrations: 0.025 μM RFC; 0.02 μM $PCNA^{AF}$; 0.1, 0.15, 0.2, or 0.4 μM ptDNA; 0.5 mM ATP; and 1 μM PCNA). Experiments with RFC mutants were performed similarly (Δt = 10 ms for RFC-B^{R84A}, Δt = 15 ms for RFC-C^{R88A}, Δt = 20 ms for RFC-D^{R101A}, and Δt = 40 ms for RFC-BCD^{AAA}) with 0.15 μM final ptDNA. The signal from four to six traces was averaged for each experiment, normalized to final value, and fit to a three-exponential function to determine PCNA secondary opening, closure, and release rates (k_5, k_8, and k_9, respectively, in the model).

ptDNA binding and release

ptDNA binding to RFC under equilibrium conditions was measured by monitoring $ptDNA^{TAMRA}$ fluorescence (λ_{ex} = 555 nm, λ_{em} = 565–590 nm) on a FluoroMax-3 fluorometer (Horiba Jobin-Yvon). $ptDNA^{TAMRA}$ (1 nM) was titrated with RFC (0–0.1 μM) in Buffer A containing BSA (0.05 mg/ml) and ATPγS (0.1 mM). Normalized peak values (λ_{em} = 582 nm) were plotted *versus* RFC concentration, and the K_D was determined by fitting the data to a quadratic equation for 1:1 binding. The kinetics of ptDNA interactions with RFC were measured by monitoring $ptDNA^{TAMRA}$ fluorescence (λ_{ex} = 550 nm, λ_{em} > 570 nm) on a stopped-flow instrument using single or double mixing schemes. ptDNA binding with ATPγS was measured by mixing RFC, PCNA, and ATPγS with $ptDNA^{TAMRA}$ (final concentrations: 0.1 μM RFC, 0.4 μM PCNA, 0.02 μM $ptDNA^{TAMRA}$,

and 100 μM ATPγS). ptDNA binding with ATP was measured by first mixing RFC and PCNA with ATP (Δt = 3 s to allow PCNA opening) followed by mixing with ptDNA^{TAMRA} (final concentrations: 0.08, 0.1, or 0.15 μM RFC; 0.4 μM PCNA; 0.02 μM ptDNA^{TAMRA}; and 0.5 mM ATP). The signal from four to six traces was averaged for each experiment, normalized to initial value, and fit to a two-exponential function to determine ptDNA binding and positioning rates (k_4 and k_5, respectively, in the model). ptDNA binding and release were measured by first mixing RFC, PCNA, and ATP with ptDNA^{TAMRA} and ATP (Δt = 10 ms for RFC and RFC-B^{R84A}, Δt = 15 ms for RFC-C^{R88A}, Δt = 20 ms for RFC-D^{R101A}, and Δt = 40 ms for RFC-BCD^{AAA} to allow ptDNA binding) followed by mixing with excess unlabeled ptDNA chase and ATP (final concentrations: 0.15 μM RFC, 0.4 μM PCNA, 0.02 μM ptDNA^{TAMRA}, 0.5 mM ATP, and 1 μM ptDNA). The signal from four to six traces was averaged for each experiment, normalized to final value, and fit to a two-exponential function to determine ptDNA positioning and release rates (k_5 and k_8, respectively, in the model).

Phosphate release

Phosphate (P_i) release from RFC after ATP hydrolysis was measured by monitoring P_i-binding reporter PBP^{MDCC} fluorescence (λ_{ex} = 425 nm, λ_{em} > 450 nm) under pre-steady-state conditions on a stopped-flow instrument using a double mixing scheme. RFC and PCNA were first mixed with ATP (Δt = 3 s to allow PCNA opening) followed by mixing with ptDNA, ssDNA (40-nt primer), or dsDNA (40-nt primer/complement) and PBP^{MDCC} in buffer containing a P_i contaminant-mopping system of 0.1 unit/ml polynucleotide phosphorylase (Sigma-Aldrich) and 0.2 mM 7-methylguanosine (R.I. Chemical Inc., Orange, CA) (final concentrations: 0.5 μM RFC, 1 μM PCNA, 2.5 μM DNA, 0.5 mM ATP, and 10 μM PBP^{MDCC}). The signal from four to six traces was averaged for each experiment and converted to P_i concentration using a calibration curve generated with standard P_i solution (Sigma-Aldrich). A small amount of P_i formed during Δt was subtracted (<10% of burst amplitude), and the data were fit to an exponential + linear function for initial estimate of the P_i release rate and the steady-state ATPase rate (k_{cat} = linear slope/3 × [RFC]).

Author contributions—Y. Z. helped conceive the project, generated RFC mutants, and performed initial exploratory experiments. J. L. developed the project, refined assays, performed experiments, analyzed and interpreted data, and crafted the manuscript. M. M. H. conceived and supervised the project, analyzed and interpreted data, and crafted the manuscript.

Acknowledgments—We thank Linda Bloom for PCNA clones, Siying Chen for ATPase data with dsDNA, Brian Kelch for interpretation of structural data, and Miho Sakato for discussions about experiments.

References

1. O'Donnell, M., Langston, L., and Stillman, B. (2013) Principles and concepts of DNA replication in bacteria, archaea, and eukarya. *Cold Spring Harb. Perspect. Biol.* **5,** a010108
2. Johnson, A., and O'Donnell, M. (2005) Cellular DNA replicases: components and dynamics at the replication fork. *Annu. Rev. Biochem.* **74,** 283–315
3. Kelch, B. A. (2016) Review: The lord of the rings: structure and mechanism of the sliding clamp loader. *Biopolymers* **105,** 532–546
4. Kelch, B. A., Makino, D. L., O'Donnell, M., and Kuriyan, J. (2012) Clamp loader ATPases and the evolution of DNA replication machinery. *BMC Biol.* **10,** 34
5. Boehm, E. M., Gildenberg, M. S., and Washington, M. T. (2016) The many roles of PCNA in eukaryotic DNA replication. *Enzymes* **39,** 231–254
6. Choe, K. N., and Moldovan, G. L. (2017) Forging ahead through darkness: PCNA, still the principal conductor at the replication fork. *Mol. Cell* **65,** 380–392
7. De March, M., Merino, N., Barrera-Vilarmau, S., Crehuet, R., Onesti, S., Blanco, F. J., and De Biasio, A. (2017) Structural basis of human PCNA sliding on DNA. *Nat. Commun.* **8,** 13935
8. Krishna, T. S., Kong, X. P., Gary, S., Burgers, P. M., and Kuriyan, J. (1994) Crystal structure of the eukaryotic DNA polymerase processivity factor PCNA. *Cell* **79,** 1233–1243
9. Georgescu, R. E., Kim, S. S., Yurieva, O., Kuriyan, J., Kong, X. P., and O'Donnell, M. (2008) Structure of a sliding clamp on DNA. *Cell* **132,** 43–54
10. Moarefi, I., Jeruzalmi, D., Turner, J., O'Donnell, M., and Kuriyan, J. (2000) Crystal structure of the DNA polymerase processivity factor of T4 bacteriophage. *J. Mol. Biol.* **296,** 1215–1223
11. Jeruzalmi, D., O'Donnell, M., and Kuriyan, J. (2001) Crystal structure of the processivity clamp loader γ complex of *E. coli* DNA polymerase III. *Cell* **106,** 429–441
12. Bowman, G. D., O'Donnell, M., and Kuriyan, J. (2004) Structural analysis of a eukaryotic sliding DNA clamp-clamp loader complex. *Nature* **429,** 724–730
13. Kelch, B. A., Makino, D. L., O'Donnell, M., and Kuriyan, J. (2011) How a DNA polymerase clamp loader opens a sliding clamp. *Science* **334,** 1675–1680
14. Bloom, L. B. (2009) Loading clamps for DNA replication and repair. *DNA Repair* **8,** 570–578
15. Sakato, M., Zhou, Y., and Hingorani, M. M. (2012) ATP binding and hydrolysis-driven rate-determining events in the RFC-catalyzed PCNA clamp loading reaction. *J. Mol. Biol.* **416,** 176–191
16. Zhou, Y., and Hingorani, M. M. (2012) Impact of individual proliferating cell nuclear antigen-DNA contacts on clamp loading and function on DNA. *J. Biol. Chem.* **287,** 35370–35381
17. Chen, S., Levin, M. K., Sakato, M., Zhou, Y., and Hingorani, M. M. (2009) Mechanism of ATP-driven PCNA clamp loading by *S. cerevisiae* RFC. *J. Mol. Biol.* **388,** 431–442
18. Marzahn, M. R., Hayner, J. N., Meyer, J. A., and Bloom, L. B. (2015) Kinetic analysis of PCNA clamp binding and release in the clamp loading reaction catalyzed by *Saccharomyces cerevisiae* replication factor C. *Biochim. Biophys. Acta* **1854,** 31–38
19. Kumar, R., Nashine, V. C., Mishra, P. P., Benkovic, S. J., and Lee, T. H. (2010) Stepwise loading of yeast clamp revealed by ensemble and single-molecule studies. *Proc. Natl. Acad. Sci. U.S.A.* **107,** 19736–19741
20. Ason, B., Handayani, R., Williams, C. R., Bertram, J. G., Hingorani, M. M., O'Donnell, M., Goodman, M. F., and Bloom, L. B. (2003) Mechanism of loading the *Escherichia coli* DNA polymerase III β sliding clamp on DNA. *Bona fide* primer/templates preferentially trigger the gamma complex to hydrolyze ATP and load the clamp. *J. Biol. Chem.* **278,** 10033–10040
21. Anderson, S. G., Thompson, J. A., Paschall, C. O., O'Donnell, M., and Bloom, L. B. (2009) Temporal correlation of DNA binding, ATP hydrolysis, and clamp release in the clamp loading reaction catalyzed by the *Escherichia coli* γ complex. *Biochemistry* **48,** 8516–8527
22. Paschall, C. O., Thompson, J. A., Marzahn, M. R., Chiraniya, A., Hayner, J. N., O'Donnell, M., Robbins, A. H., McKenna, R., and Bloom, L. B. (2011) The *Escherichia coli* clamp loader can actively pry open the β-sliding clamp. *J. Biol. Chem.* **286,** 42704–42714
23. Hayner, J. N., and Bloom, L. B. (2013) The β sliding clamp closes around DNA prior to release by the *Escherichia coli* clamp loader γ complex. *J. Biol. Chem.* **288,** 1162–1170
24. Alley, S. C., Abel-Santos, E., and Benkovic, S. J. (2000) Tracking sliding clamp opening and closing during bacteriophage T4 DNA polymerase holoenzyme assembly. *Biochemistry* **39,** 3076–3090

25. Trakselis, M. A., Berdis, A. J., and Benkovic, S. J. (2003) Examination of the role of the clamp-loader and ATP hydrolysis in the formation of the bacteriophage T4 polymerase holoenzyme. *J. Mol. Biol.* **326,** 435–451
26. Zhuang, Z., Berdis, A. J., and Benkovic, S. J. (2006) An alternative clamp loading pathway via the T4 clamp loader gp44/62-DNA complex. *Biochemistry* **45,** 7976–7989
27. Marzahn, M. R., Hayner, J. N., Finkelstein, J., O'Donnell, M., and Bloom, L. B. (2014) The ATP sites of AAA+ clamp loaders work together as a switch to assemble clamps on DNA. *J. Biol. Chem.* **289,** 5537–5548
28. Chiraniya, A., Finkelstein, J., O'Donnell, M., and Bloom, L. B. (2013) A novel function for the conserved glutamate residue in the walker B motif of replication factor C. *Genes* **4,** 134–151
29. Miller, J. M., and Enemark, E. J. (2016) Fundamental characteristics of AAA+ protein family structure and function. *Archaea* **2016,** 9294307
30. Sakato, M., O'Donnell, M., and Hingorani, M. M. (2012) A central swivel point in the RFC clamp loader controls PCNA opening and loading on DNA. *J. Mol. Biol.* **416,** 163–175
31. Simonetta, K. R., Kazmirski, S. L., Goedken, E. R., Cantor, A. J., Kelch, B. A., McNally, R., Seyedin, S. N., Makino, D. L., O'Donnell, M., and Kuriyan, J. (2009) The mechanism of ATP-dependent primer-template recognition by a clamp loader complex. *Cell* **137,** 659–671
32. Adelman, J. L., Chodera, J. D., Kuo, I. F., Miller, T.F., 3rd, and Barsky, D. (2010) The mechanical properties of PCNA: implications for the loading and function of a DNA sliding clamp. *Biophys. J.* **98,** 3062–3069
33. Kazmirski, S. L., Zhao, Y., Bowman, G. D., O'donnell, M., and Kuriyan, J. (2005) Out-of-plane motions in open sliding clamps: molecular dynamics simulations of eukaryotic and archaeal proliferating cell nuclear antigen. *Proc. Natl. Acad. Sci. U.S.A.* **102,** 13801–13806
34. Millar, D., Trakselis, M. A., and Benkovic, S. J. (2004) On the solution structure of the T4 sliding clamp (gp45). *Biochemistry* **43,** 12723–12727
35. Tainer, J. A., McCammon, J. A., and Ivanov, I. (2010) Recognition of the ring-opened state of proliferating cell nuclear antigen by replication factor C promotes eukaryotic clamp-loading. *J. Am. Chem. Soc.* **132,** 7372–7378
36. Yao, N. Y., Johnson, A., Bowman, G. D., Kuriyan, J., and O'Donnell, M. (2006) Mechanism of proliferating cell nuclear antigen clamp opening by replication factor C. *J. Biol. Chem.* **281,** 17528–17539
37. Goedken, E. R., Kazmirski, S. L., Bowman, G. D., O'Donnell, M., and Kuriyan, J. (2005) Mapping the interaction of DNA with the *Escherichia coli* DNA polymerase clamp loader complex. *Nat. Struct. Mol. Biol.* **12,** 183–190
38. Story, R. M., and Steitz, T. A. (1992) Structure of the recA protein-ADP complex. *Nature* **355,** 374–376
39. Thompson, J. A., Marzahn, M. R., O'Donnell, M., and Bloom, L. B. (2012) Replication factor C is a more effective proliferating cell nuclear antigen (PCNA) opener than the checkpoint clamp loader, Rad24-RFC. *J. Biol. Chem.* **287,** 2203–2209
40. Zhuang, Z., Yoder, B. L., Burgers, P. M., and Benkovic, S. J. (2006) The structure of a ring-opened proliferating cell nuclear antigen-replication factor C complex revealed by fluorescence energy transfer. *Proc. Natl. Acad. Sci. U.S.A.* **103,** 2546–2551
41. Hingorani, M. M., and Coman, M. M. (2002) On the specificity of interaction between the *Saccharomyces cerevisiae* clamp loader replication factor C and primed DNA templates during DNA replication. *J. Biol. Chem.* **277,** 47213–47224
42. Johnson, K. A. (2009) Fitting enzyme kinetic data with KinTek Global Kinetic Explorer. *Methods Enzymol.* **467,** 601–626
43. Miyata, T., Suzuki, H., Oyama, T., Mayanagi, K., Ishino, Y., and Morikawa, K. (2005) Open clamp structure in the clamp-loading complex visualized by electron microscopic image analysis. *Proc. Natl. Acad. Sci. U.S.A.* **102,** 13795–13800
44. Tondnevis, F., Weiss, T. M., Matsui, T., Bloom, L. B., and McKenna, R. (2016) Solution structure of an "open" *E. coli* Pol III clamp loader sliding clamp complex. *J. Struct. Biol.* **194,** 272–281
45. Williams, C. R., Snyder, A. K., Kuzmic, P., O'Donnell, M., and Bloom, L. B. (2004) Mechanism of loading the *Escherichia coli* DNA polymerase III sliding clamp. I. Two distinct activities for individual ATP sites in the γ complex. *J. Biol. Chem.* **279,** 4376–4385
46. Finkelstein, J., Antony, E., Hingorani, M. M., and O'Donnell, M. (2003) Overproduction and analysis of eukaryotic multiprotein complexes in *Escherichia coli* using a dual-vector strategy. *Anal. Biochem.* **319,** 78–87
47. Brune, M., Hunter, J. L., Howell, S. A., Martin, S. R., Hazlett, T. L., Corrie, J. E., and Webb, M. R. (1998) Mechanism of inorganic phosphate interaction with phosphate binding protein from *Escherichia coli*. *Biochemistry* **37,** 10370–10380